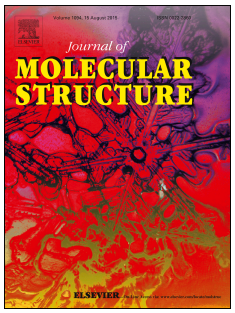

An analysis of structural, spectroscopic signatures, reactivity and anti-bacterial study of synthetized 4-chloro-3-sulfamoylbenzoic acid

Ch Kavitha, K. Narendra, A. Ratnakar, Nuthalapati Poojith, C. Sampath, Subrata Banik, P.A. Suchetan, Krishna Murthy Potla, Nuthalapati Venkatasubba Naidu

PII: S0022-2860(19)31285-2

DOI: https://doi.org/10.1016/j.molstruc.2019.127176

Reference: MOLSTR 127176

To appear in: *Journal of Molecular Structure*

Received Date: 24 June 2019

Revised Date: 19 September 2019

Accepted Date: 1 October 2019

Please cite this article as: C. Kavitha, K. Narendra, A. Ratnakar, N. Poojith, C. Sampath, S. Banik, P.A. Suchetan, K.M. Potla, N.V. Naidu, An analysis of structural, spectroscopic signatures, reactivity and anti-bacterial study of synthetized 4-chloro-3-sulfamoylbenzoic acid, *Journal of Molecular Structure* (2019), doi: https://doi.org/10.1016/j.molstruc.2019.127176.

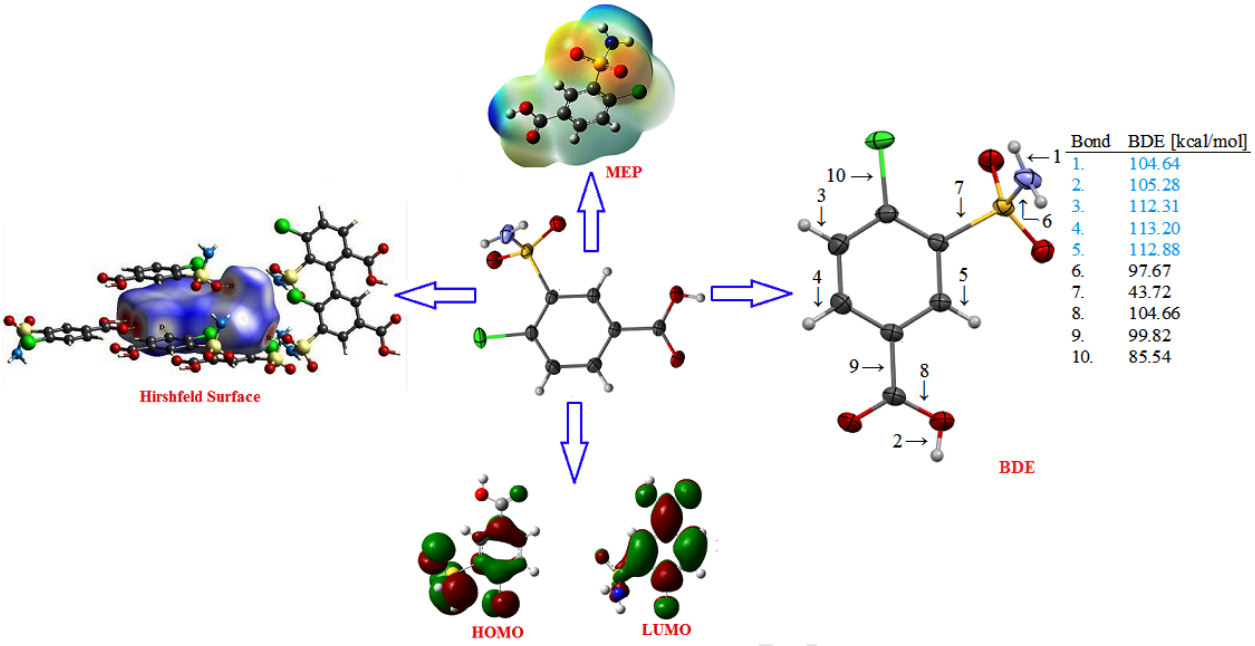

Bond	BDE [kcal/mol]
1.	104.64
2.	105.28
3.	112.31
4.	113.20
5.	112.88
6.	97.67
7.	43.72
8.	104.66
9.	99.82
10.	85.54

An analysis of structural, spectroscopic signatures, reactivity and anti-bacterial study of synthetized 4-chloro-3-sulfamoylbenzoic acid

Ch. Kavitha[a], K. Narendra[b], A. Ratnakar[a], Nuthalapati Poojith[c], C. Sampath[d], Subrata Banik[e], P.A. Suchetan[f], Krishna Murthy Potla[g*], Nuthalapati Venkatasubba Naidu[h]

[a]Department of Chemistry, Velagapudi Ramakrishna Siddhartha Engineering College, Vijayawada-520007, A.P., India.

[b]Department of Physics, Velagapudi Ramakrishna Siddhartha Engineering College, Vijayawada -520007, A.P., India.

[c]Sri Ramachandra Institute of Higher Education and Research, Ramachandra Nagar, Porur, Chennai-600 116.

[d]Department of Chemistry, B.M.S. College of Engineering, Bull Temple Road, Bengaluru-560 019, India

[e]School of Chemistry, University of Hyderabad, Hyderabad, 500046, India

[f]Department of Studies and Research in Chemistry, University College of Science, Tumkur University, Tumkur-572 103, Karnataka, India.

[g]Department of Chemistry, Bapatla Engineering College, Acharya Nagarjuna University Post Graduate Research Centre, Bapatla-522 102, A.P., India.

[h]Department of Chemistry, Sri Venkateswara University, Tirupati-517 502.

*Corresponding author: Dr. Krishna Murthy Potla (krishnamurthypotla@gmail.com)

Abstract

In the current study, 4-chloro-3-sulfamoylbenzoic acid (CSBA) has been synthetized from 4-chloro-3-sulfamoylbenzoate. The explicit structure of the titled compound was authenticated by single crystal X-ray diffraction, vibrational and electronic spectroscopic signatures. The unambiguous structure in solid state was confirmed by single crystal X-ray diffraction technique and Hirshfeld surface analysis. The X-ray analysis reflect that the titled compound was crystallized in monoclinic crystal system with $P2_1/c$ space group a = 4.9576(3) Å, b = 6.0315(3) Å, c = 29.8923(16) Å, β = 92.628(3)°, volume = 892.89(8) Å^3 and Z = 4. In the solid phase structure, the molecules were interconnected by O-H…O and N-H…O hydrogen bonds and C-H…O intermolecular interactions forming a two dimensional sheet. These contacts were further

envisaged by 3D-hirshfeld surface studies (d_{norm}) and 2D-fingerprint plots; which suggested that the O---H(39.9%) contact contributed the highest to the surface. The molecular, vibrational and electronic properties of titled compound investigated by using quantum chemical calculations at DFT/B3LYP/6-311+G(d,p) level of theory. An analysis each fundamental vibrational mode was performed with the help of potential energy distribution (PED) using VEDA4 program. In addition, frontier orbital analysis, global reactivity parameters, natural bond order (NBO) analysis, non-linear optical (NLO) calculation and molecular electrostatic potential (MEP) analysis were performed by same method in same phase. Bond dissociation energies have been calculated for all single acyclic bonds in order to study autoxidation mechanism and degradation properties of the present investigated molecule. The titled compound displayed moderate anti-bacterial activity against gram-positive and gram-negative bacteria.

Key words: sulfamoylbenzoic acid; BDE; Fukui reactive index; SCXRD studies; anti-bacterial studies

1. Introduction

Sulfa-drugs (sulfonamides) are promising chemotherapeutic agents containing SO_2-NH group as a key functional group. The findings of sulfonamides is an important milestone event in the human chemotherapeutic account. Sulfonamides and their derivatives have attracted intense interest due to their useful biological and pharmacological properties, such as Alzheimer's [1], HIV [2], cancer [3, 4], rheumatoid arthritis [5], anti-inflammatory [6], carbonic anhydrase inhibitor [7], insecticidal [8], anti-protozoal [9], anti-fungal [10] and anti-bacterial [11]. Besides pharmaceutical applications, sulfonamides are also used as reagents in analytical chemistry for concentration, separation, selective qualitative and quantitative determination of the 3d transition metal cations [12-14].

Sulfonamide compounds have been studied extensively and numerous experimental and computational reports. Gowda *et al.,* [15] reported Infrared and NMR spectra of 4-chlorobenzenesulfonamide (I), 4-bromobenzenesulfonamide (II), 4- and 4-fluorobenzenesulfonamide (III), and they have also analyzed X-ray crystallographic structure of these aryl sulfonamides [16]. Karabacak *et al.,* [17] analyzed theoretical investigation on the molecular structure, infrared, Raman and NMR spectra of *para*-halogen benzene sulfonamides, 4-X-$C_6H_4SO_2NH_2$ (X=Cl, Br or F).

K. Govindarasu *et al.,* [18] reported Synthesis, structural, spectroscopic studies, NBO analysis, NLO and HOMO-LUMO of N-phenyl benzene sulfonamide by experimental and theoretical approaches. S. Murugavel *et al.,* [19, 20] analyzed synthesis, crystal structure analysis, spectral investigations, DFT computations, biological activities and molecular docking studies of sulfonamide derivative compounds. Vega-Hissi *et al.,* carried out detailed theoretical studies on sulphanilamide and its derivatives within the Hartree-Fock and density functional approaches [21].

By keeping in view of the importance and applications of sulfonamide moieties, we have accomplished synthesis, Hirshfeld surface analysis and experimental spectroscopic characterization of the 4-chloro-3-sulfamoylbenzoic acid (CSBA) molecule with computational study by DFT. To the best of our knowledge, there were no reports on crystal structure analysis, Hirshfeld surface analysis and computational studies. The synthetized compound was distinctively characterized by SCXRD, FT-IR and FT-Raman spectroscopic techniques. Spectral data were also computed within DFT method in order to validate the used level of theory. Computational studies within DFT method have demonstrated to be an effective tool for the analysis of physical and chemical properties of various organic compounds [22-25] and in this study, we used it to analyze both the global reactivity parameters and local quantum-molecular descriptors of the molecule. Furthermore, Fukui functions, bond dissociation energy calculations and anti-bacterial activity studies were performed for the synthetized molecule. In this contribution, we herein disclose an analysis of structural, spectroscopic signatures, reactivity and anti-bacterial study of synthetized 4-chloro-3-sulfamoylbenzoic acid.

2. Experimental methods

2.1. General

All chemical and solvents used for the synthesis were procured from commercial source. Fourier transformed Infrared (FT-IR) spectrum (Fig. 1.) was recorded in Perkin Elmer Spectrum 1 FT-IR spectrometer scan range from 450-4000 cm^{-1} with resolution 1.0 cm^{-1} by KBr pellets method. Fourier transformed Raman spectrum (Fig. 2.) was recorded in Bruker 27: Standalone FT-Raman spectrometer by using Nd:YAG laser source (wavelength: 1064 nm) with 2.0 cm^{-1} resolution in the range 50-4000 cm^{-1}. ^{1}H-NMR spectrum was recorded in Bruker 400MHz spectrometer using DMSO-d_6 as a solvent and tetramethylsilane (TMS) as an internal standard.

2.2. Synthesis of 4-chloro-3-sulfamoylbenzoic acid

To a 50 mL round-bottomed flask, methyl-4-chloro-3-sulfamoylbenzoate (800 mg, 3.20 mmol) was dissolved in tetrahydrofuran (8 mL) and the reaction mixture was cooled to 0ºC. To this reaction mixture, an aqueous solution of 10 % lithium hydroxide (223 mg, 9.6 mmol) was added and stirred for 2 h at room temperature. After completion of the reaction, the reaction mixture was evaporated under reduced pressure and the aqueous layer was acidified with 6N hydrochloric acid. Then the precipitate was filtered and dried under vacuum to afford a white solid (610 mg, yield: 81.3 %) 4-chloro-3-sulfamoylbenzoic acid (Scheme -1). Recrystallization has been carried out in ethyl acetate: dry ethyl ether (3:1) solution by slow evaporation crystal growth technique at ambient temperature.

^{1}H-NMR (400 MHz, DMSO-d_6) δ: 13.60 (s, 1H, COOH), 8.51 (d, J = 2.0 Hz, 1H, Ph-H), 8.10 (dd, J = 8.2, 2.1 Hz, 1H, Ph-H), 7.82 (s, 2H, SO_2NH_2), 7.79 (d, J = 8.3 Hz, 1H, Ph-H).

2.3.X-ray crystallography studies

A colourless and needle shaped single crystal of the titled compound, with dimensions of 0.24 mm × 0.22 mm × 0.19 mm was selected and mounted on a Bruker APEX-II CCD diffractometer with monochromated MoKα radiation (λ = 0.71073 Å) at 296(2) K. The data was processed with SAINT and corrected for absorption using SADABS [26]. The structure was solved by direct method using the program SHELXL [27] and was refined by full-matrix least squares technique on F^2 using anisotropic displacement parameters for all non-hydrogen atoms. The carbon-bound H atoms were placed in calculated positions (C_{arom}-H= 0.93 Å and $C_{methylene}$-H= 0.97 Å) and were included in the refinement in the riding-model approximation, with U_{iso} (H) set to 1.2U_{eq} (C). The oxygen and nitrogen bound H atoms were located from difference-Fourier maps and refined as riding: O-H = 0.82 Å and N-H = 0.86 Å.

2.4. Computational tools

The quantum chemical calculations for 4-chloro-3-sulfamoylbenzoic acid were performed using density functional theory with three parameter hybrid functional B3LYP with 6-311+(d,p) basis set, and in calculating nonlinear optical properties we use CAM-B3LYP/6-311+(d). All the calculations are performed using Gaussian09 software [28] and the examination of inputs/results were performed through GaussView [29]. Initial geometry of the investigated compound was extracted from single crystal X-ray coordinates. The computed wave numbers were scaled with 0.9613 to attain a good correlation with experimental wave numbers [30]. In addition, frontier

orbital analysis, global reactivity descriptors, NBO analysis, NLO calculations, BDE calculations, MEP analysis and atomic charge analysis were performed by same method.

2.5. Hirshfeld surface analysis

3D-Hirshfeld surfaces [31-33] associated 2D-finger print analysis [34-36] was carried out for CSBA compound by using powerful graphical tool CrystalExplorer3.1 software [37], which accept CIF as the input file.

3. Results and discussion

3.1. Crystal structure and Hirshfeld surface analysis

The *ORTEP* diagram for the CSBA compound was given in Fig. 3, the interactions and packing of molecules in the crystal lattice was shown in Fig. 4(a) and Fig. 4(b). The crystallographic data and refinement parameters were summarized in Table 1. Geometric parameters for hydrogen bonds and other intermolecular contacts (Å, °) operating in the crystal structures were listed in Table 2.

The crystal structure of the titled compound can be explained in terms of the supramolecular aggregation of the molecules first via strong hydrogen bonds followed by moderate or weaker intermolecular interactions. The molecules are first interconnected via strong O-H…O hydrogen bonds, namely O5-H18…O3, to form a $R^2_2(8)$ dimeric motif. These inversion-related dimers are extended into a one dimensional ribbon, wherein, the equivalent molecules are connected by two anti-parallel C(6) chains of N4-H19…O7 hydrogen bonds. The adjacent ribbons are further interlinked via another N-H…O hydrogen bond, namely N4-H20…O7. The C(6) chains of N4-H20…O7 hydrogen bonds connect the 2-fold related molecules in the adjacent ribbons resulting in a complex zig-zag two dimensional architecture. A complex three dimensional grid like architecture is ensued via C15-H16…O5 interactions that interlink the molecules forming C(6) chains. Thus, the two N-H…O hydrogen bonds and the C-H…O interactions have structure directing characteristics- the former two extending a zero dimensional architecture to a two dimensional structure, while, the later extending the two dimensional structure into a three dimensional one.

The Hirshfeld surfaces for CSBA compound illustrated in Fig. 5(a), showing surfaces that have been mapped over a d_{norm} (1) *shape index* (2) *curvedness* (3) and *fragment patch* (4) range of -0.7311 to 1.0450 Å, -1.00 to 1.00 Å, -4.00 to 0.400 Å and 0.00 to 12.00 Å, respectively. In Fig. 5(b), the bright red spots are the hydrogen bonding centers O5-H18…O3, N4-H19…O7 and N4-

H20…O7 labeled as A, B and C, respectively. The other region which was pale red in colour showed weak C15-H16…O5 intermolecular interaction marked as D on d_{norm} surface.

The relative contribution of the various interactions on the Hirshfeld surface was accounted for the CSBA compound by fingerprint analysis. The fingerprint analysis reflection shown that the O---H contacts can account for about 39.9 % of the total Hirshfeld surface area and these interactions appeared as two distinct spikes of almost equal length (see in Fig.5(c)). The upper spikes corresponds to donor spikes (hydrogen atom of acid group interact with oxygen atom of acid group and hydrogen atom of sulfonamide group interact with oxygen atom of sulfonamide group), while lower spikes corresponds to acceptor spikes (oxygen atom of acid group interact with hydrogen atom of acid group, oxygen atom of sulfonamide group interact with hydrogen atom of sulfonamide group and oxygen atom of acid group interact with hydrogen atom of benzene ring); the remaining contribution were mostly due to H---H (16.9%), Cl---O (7.4%), Cl---C (4.7%) and C---C (3.5%) interactions, with only minor contribution from other O---O(1.7 %), Cl---N(1.7 %) and N---H (0.9 %) interactions.

3.2.Optimization of geometry

The optimization of CSBA compound (Fig. 3) performed at DFT/B3LYP/6-311G+(d,p) level of theory. The optimized structures for CSBA compound possess C1point group with ground state energy -1484.5762 a.u. Selected geometrical parameters bond length (Å), bond angle (º) and torsion angle (º) of CSBA compound were outlined in Table 3. The C-C bond lengths (DFT/XRD) of aromatic ring in the titled compound were in the range 1.3875-1.3998/1.378-1.396 Å and for the benzene ring the C-C bond length was 1.3993 Å [38]. The bond length of sulfonamide group were S_2-O_7 = 1.45235/1.4374 Å, S_2-O_6 = 1.45598/1.4258 Å, S_2-N_4 = 1.66847/1.5884 Å, S_2-C_{12} = 1.82275/ 1.78 Å are close to the reported values S_2-O_7 = 1.457/1.435 Å, S_2-O_6 = 1.456/1.423 Å, S_2-N_4 = 1.706/1.636 Å, S_2-C_{12} = 1.794/1.756 Å [39]. For the carboxylic group (DFT/XRD) C_8-O_3 = 1.20772/1.252 Å, C_8-O_5 = 1.35213/1.273 Å, O_5-H_{18} = 0.96872/0.8185 Å. Murthy et al. [40] reported (DFT/XRD) C_8-O_3 = 1.201/1.208 Å, C_8-O_5 = 1.359/1.304 Å, O_5-H_{18} = 0.96749/0.886 Å. The C_{17}-Cl_1 bond length (DFT/XRD) is 1.75083/1.720 Å which was in good agreement with reported values [41]. At C_{17}, the bond angle (DFT/XRD) C_{12}-C_{17}-C_{15} was 120.3/120.1º and this enhancement of bond angle from 120º was due to the presence of electronegative atom Cl_1. At C8 position the bond angles were, C_9-C_8-O_5 112.8/117.6º, O_3-C_8-O_5 122.8/123.2º, C_9-C_8-O_3 124.3/119.1º and the asymmetry in these angles

unveil the interaction between carbonyl groups and hydroxyl groups and thereby, supporting the existence of intermolecular hydrogen between two acid groups of CSBA compound. The sulfonyl bound benzene (C_{10}-C_{12}-C_{17}) ring also appears to be a little distorted because of the SO_2 group substituted at C12 position seen from the bond angle C_{10}-C_{12}-C_{17} (119.4º by DFT/XRD) value which was lesser than typical hexagonal angle of 120º.

3.3.Vibrational analysis

The calculated (scaled) wave numbers, experimental IR, Raman bands and assignments were given in Table 4. The carboxylic group was characterized by the OH stretch, C=O stretch and OH out-of-plane deformation and by the C-O stretch and OH in-plane deformation. Wherein, the OH stretching mode showed a band at 3623 cm^{-1} theoretically with IR intensity 125.1003, Raman activity 157.5832 and a PED of 100 %. For the titled compound, carboxyl group C=O stretching vibrational mode displayed a band at 1721 cm^{-1} (IR), 1720 cm^{-1} (Raman), 1722 cm^{-1} (DFT) with IR intensity 423.2576, Raman activity 138.0385 and a PED of 84 % which was expected in the region 1750-1600 cm^{-1} [42,43]. The C=O in-plane deformations were expected in the region 625±70 cm^{-1} [42]. The bands at 676, 641 cm^{-1} in the IR spectrum, 675 cm^{-1} in the Raman spectrum and 674, 646 cm^{-1} (DFT) were assigned as C=O in-plane deformation modes. The O-H in-plane deformation, coupled to the C=O stretching mode was expected in the region 1390±55 cm^{-1} [44], and the band at 1313 cm^{-1} in the IR spectrum, 1310 cm^{-1} in the Raman spectrum and 1315 cm^{-1} (DFT) was assigned to the stretching vibration of the O_5-H_{18} group.

The vibration modes associated with NH_2 group were expected in the regions, 3300-3540 cm^{-1} (stretching), 1580-1640 cm^{-1}, 1100-1300 cm^{-1} and 585-710 cm^{-1} (deformation modes) respectively [42]. The NH_2 group asymmetric stretching mode assigned to 3401 cm^{-1} (IR), 3403 cm^{-1} (Raman), 3495 cm^{-1} (DFT) with 44.9905 IR intensity, 28.6368 Raman activity and a PED of 50 % (mode no 2) and symmetric stretching mode assigned at 3281 cm^{-1} (IR), 3279 cm^{-1} (Raman), 3383 cm^{-1} (DFT) with 32.8958 IR intensity, 91.3757 Raman activity and a PED of 50 % (mode no 3). The difference in calculated and experimental N-H vibrational values were 94 (IR spectrum), 102 (Raman spectrum) owing to N-H---O interactions in solid state. For the CSBA compound, NH_2 group deformation modes were assigned for 1042, 587 cm^{-1} (IR), 1518, 1043, 585 cm^{-1} (Raman), 1520, 1041, 587 cm^{-1} (DFT), which were in concordance with reported values.

For the CSBA compound, the bands at 1284 cm^{-1} (IR), 1285 cm^{-1} (Raman), 1286cm^{-1} (DFT) and 1090, 1072 cm^{-1} (Raman), 1090, 1071 cm^{-1} (DFT) were assigned as asymmetric and symmetric stretching vibrational mode of SO_2 group, which was expected in the region 1330-1295 cm^{-1} and 1150-1125 cm^{-1}, respectively [42]. The deformation modes of SO_2 group were expected in the regions, scissoring 560±40 cm^{-1}, wagging 500±55 cm^{-1} and twisting 440±50 cm^{-1} [42]. These modes were observed at 514, 458, 430, 389 cm^{-1} (experimentally) and calculated at 513, 460, 432, 393 cm^{-1} respectively.

The stretching vibrational modes of SN group assigns to 785 cm^{-1} in the Raman spectrum and at 782 cm^{-1} theoretically and with a PED of 56 % as expected [42]. The mode calculated at 825 cm^{-1} with 74.4512 IR intensity, 18.1962 Raman activity and a PED of 15 % was assigned for CS stretching vibrational mode of CSBA compound as expected [42]. In the present case, the band at 548 cm^{-1} in the IR spectrum, 551 cm^{-1} in the Raman spectrum and 550 cm^{-1} (DFT) with IR intensity 45.1653, Raman activity 2.1073 and a PED of 17 % was assigned for C-Cl stretching mode which was expected in the region 710-505 cm^{-1} [42].

In the poly substituted aromatic rings, the C-H stretching modes showed absorbance between 3000-3100 cm^{-1} [45, 46] and DFT calculation gives these modes at 3096, 3086, 3073 cm^{-1} and experimentally modes were observed at 3093, 3072 cm^{-1} in the IR spectrum, 3084 cm^{-1} in the Raman spectrum. The aromatic ring stretching modes were calculated in the range 1562-1119 cm^{-1} and experimentally modes were observed in the range 1563-116 cm^{-1} as expected [42]. Previous literature [40], the ring breathing mode of 1,2,4 substituted phenyl ring is assigned at 1003 cm^{-1} (DFT) with PED 27 % with moderate Raman activity and low IR activity. The in-plane and out-of-plane CH deformation bands were expected in the range 1000-1300 cm^{-1} and 750-1000cm^{-1}, respectively [42] and for the CSBA compound, these modes were observed at 1352, 1145, 1115 cm^{-1} (IR), 1351, 1116 cm^{-1} (Raman), 1354, 1230, 1155, 1119 cm^{-1} (DFT) (in-plane deformation), 832, 745 (IR), 833, 747 cm^{-1} (Raman), 956, 831, 749 cm^{-1} (DFT) (out-of-plane deformation).

3.4.Natural bond orbital (NBO) analysis

The natural bond orbital (NBO) analysis were performed using NBO 3.1 program [47] as executed in the Gaussian09 program at the DFT/B3LYP/6-311+G(d,p) method, which propose a suitable basis for examining the hyper conjugative interactions. The NBO method transforms delocalized molecular orbitals (MO) into a set of orbitals that are localized over the bonds as

bonding orbitals (σ, π), anti-bonding orbitals (σ^*, π^*), and effective lone pairs and higher energy Rydberg orbitals on atoms [48]. From a second order perturbation theory, the stabilization energy due to electron delocalization over the NBOs or hyperconjugation effect is obtained as

$$E^{(2)} = \frac{q_j F(i,j)^2}{\varepsilon_j - \varepsilon_i} \quad (1)$$

Here, ε_j and ε_i are the energies of j^{th} and i^{th} NBO, called as the donor and acceptor orbitals, respectively for a hyperconjugation. $F(i,j)$ and q_j are the elements of off-diagonal Fock-matrix between j^{th} and i^{th} NBOs, and electron population on j^{th} orbital, respectively [48-50]. The large $E^{(2)}$ values show the intensive interaction between electron-donors and electron-acceptors, and the extent of conjugation of the entire system.

Second order interactions obtained by natural bond orbital analysis were tabulated in Table 5 and Table 6. We report only those interactions that has stabilization energies ($E^{(2)}$) more than 10 kcal/mol. The π electrons delocalization between these bonds are evident from the $E^{(2)}$ values of electron donation from bonding π(C9-C13) orbitals to anti-bonding π^*(O3-C8), π^*(C10-C12) and π^*(C15-C17) orbitals, 21.28, 25.78 and 20.33 kcal/mol, respectively. There is electron delocalization between the π and π^* orbitals of these four bonds, and the higher values of stabilization energies indicate that. We find large hyper-conjugation stabilization ($E^{(2)}$ = 47.46 kcal/mol) due to donation of lone pair of O5 (LP(2)) to the π^*(O3-C8) orbital. This is expected due to resonance effect within the acid group. Such large value of $E^{(2)}$ comes from strong overlap between the lone pair of O5 atom and π^*(O3-C8) through the off-diagonal Fock-matrix elements (as large as 0.115), and large electron density of the lone pair NBO (1.81825) of oxygen. We do not find any significant hyperconjugation that involves NBOs with atomic orbitals from Cl, except donation from a lone pair of Cl (LP(2)) to π^*(C15-C17). Corresponding $E^{(2)}$ is 10.86 kcal/mol, and it comes from small energy difference and a moderate Fock-matrix element value. There are moderate stabilization energies due to electron delocalization within the SO_2NH_2 as can be seen from the Table 5 and 6. However, this group does not have any significant participation with the phenyl ring due to large energies of NBOs that involve the atomic orbital of sulphur. Thus, a π electron rich -COOH group is capable of donating electrons to the benzene ring and highly electronegative -Cl group can push electron towards it. The para-positioning of these two 'push-pull' groups make the molecule a potential candidate for optical material.

3.5.NLO properties

The NLO materials have key applications in the field photonic devices, optoelectronics, frequency mixing, dynamic image processing and second harmonic wave generation [51-53]. In continuation of our earlier studies [54-69], in the present study, total dipole moment (μ), anisotropy of the polarizability (Δα), average linear polarizibility (<α>), and second-order hyperpolarizibilitiy (γ) calculations were performed at DFT/CAM-B3LYP/6-311G+(d) level of theory in the case static and results were listed in Tables 7 and 8. A study was done with the asymmetric unit and the unit cell, the results with the unit cell are better than the asymmetric unit as can be seen in Table 8. In this case we will work with the results of Table 8 divided by 4, which is the number of asymmetric units of the unit cell. The total dipole moment and average linear polarizability of the titled compound were 4.48 Debye and 18.95×10^{-24} esu. For the CSBA compound, the average second-order hyperpolarizibilitiy (<γ>) was calculated and found to be 15.01×10^{-36} esu. Thus we have found that the total dipole moment of the CSBA molecule is approximately 3.27 times greater than that of Urea and the second hyperpolarizability is 3.62 times greater than that of Urea [70]. Due to a load shift for group SO2, as can be seen in Fig. 6 of the Potential Map, we can say that the z direction has a larger contribution, see α_{zz} and γ_{zzzz}.

3.6.Local reactivity calculations (Molecular electrostatic potential and Fukui functions)

Identification of molecular reactive sites (electrophilic and nucleophilic attack) as well as hydrogen-bonding interactions [71,72] of the CSBA compound has been done by molecular electrostatic potential quantum molecular descriptor is related to the electronic density and visualized by rainbow color scheme (red-white-blue). Molecular electrostatic potential for the CSBA compound depicted in Fig. 6 was calculated at B3LYP/6-311+G(d, p) level of theory. Minimal MEP values (V(r) < -6.530 a.u.) and were in near vicinities of deprotonated oxygen atoms, designating these locations possibly sensitive towards electrophilic attacks. MEP has the maximal values (V(r) >6.530 a.u.) precisely at protonated atoms of oxygen and nitrogen designating these locations as probably sensitive nucleophilic electrophilic attacks. The obtained MEP results would help in understanding intermolecular hydrogen bond O5-H18…O3, C15-H16…O5, N4-H19…O7 and N4-H20…O7 which was obtained from SCXRD analysis.

The chemical reactivities of atoms in the molecule were calculated using local reactivity descriptor, Fukui functions (FF) [73], derived from conceptual density functional theory [73]. It was defined by the change of electron density at a given point ρ(r) when an electron was added/subtracted to a molecule. Thus, it was used as a tool to identify the nucleophilic,

electrophilic and radical attack center in a molecule. Equating the electron charge on an atom in the molecule (q) to the electron density of the atom, three different types of FFs were defined to identify which atom should be more responsive towards the nucleophilic, electrophilic and radical reactions [74, 75].

$$f^{+} = [q(N+1) - q(N)]; \text{ for a nucleophilic attack,} \quad (2)$$

$$f^{-} = [q(N) - q(N-1)]; \text{ for a electrophilic attack,} \quad (3)$$

$$f^{0} = [q(N+1) - q(N-1)]/2; \text{ for a radical attack} \quad (4)$$

Different types of wave function analysis were available to obtain the charge (q). We use Hirshfeld population analysis to calculate the FF. The Fukui reactive indices were given in Table 9. Understandably, the Chlorine atom has the highest value of all the three indexes, since both HOMO and LUMO has contribution from *p*-orbitals of Chlorine atom. Similar argument holds for the higher values of f^{+}, f^{-}, and f^{0} of O_3 oxygen. Among the carbon atoms, the carbon to which Chlorine atom was attached and the carboxylic carbon (C8) were found to be effective sites for nucleophilic attack. The f^{+} values for these two centers were 0.087 and 0.080 respectively. The C9 to which the carboxylic group was attached and emerged to be the most electrophilic carbon center (f^{-} value is 0.095). The C17 carbon has the highest f^{0} value among the entire carbon centers, as expected because of high electronegative Chlorine attached to it.

3.7.Frontier Molecular Orbitals Analysis

The computation of the molecular orbitals, particularly the highest occupied molecular orbital (HOMO) and lowest unoccupied molecular orbital (LUMO) is an important tool to analyze the molecular properties and reactivities. The difference between the energies of these two orbitals, the HOMO-LUMO gap, i.e. the band gap (ΔE) is directly related to the chemical stability of a molecule, its chemical properties, spectroscopic properties and other NLO properties. From Koopmans' theory, the ionization potential of a molecule is equal to the negative of HOMO energy (EHOMO), and its electron affinity is equal to negative of LUMO energy (ELUMO).

$I = -EHOMO$ and $A = -ELUMO$. (5)

Relations with the $EHOMO$ and $ELUMO$ and ΔE have been established to calculate chemical properties like electronegativity(χ), global hardness(η), chemical softness(ν), chemical potential(μ), electrophilic index (ω) using conceptual density functional theory [75]. Unlike the

local reactivity indexes (f^+, f and f^0) that gives the account of possible reactive site of a molecule, these quantities enable us to understand the inertness and reactivity of a molecules as whole towards chemical reactions, and this known as global reactivity parameters. These quantities are calculated though the following equations [75].

$$\chi = \frac{1}{2}(I + A) = \frac{1}{2}(EHOMO + ELUMO) \quad (6)$$

$$\eta = \frac{1}{2}(ELUMO - EHOMO) \quad (7)$$

$$\mu = -\chi = -\frac{1}{2}(EHOMO + ELUMO) \quad (8)$$

$$S = 1/\eta \quad (9)$$

$$\omega = \mu 2/2\eta \quad (10)$$

The pictorial representation of frontier orbitals for the titled molecule is shown in Fig. 7. HOMO (MO 60, -7.9556 eV) was localized over whole molecule other than acid group and LUMO (MO 61, -2.5730 eV) was spread over whole molecule other than amine group and this reflect that there was a charge transfer from amine group to acid group and energy gap between frontier orbitals is 5.3826 eV. The global reactivity parameters for present titled molecule are: ionization potential I = 7.9556 eV, electron affinity A = 2.5730 eV, electronegativity χ = 5.2643 eV, global hardness η = 2.6913 eV, chemical potential μ = 5.2643 eV, Chemical softness ν = 0.3715 eV and electrophilicity index ω = 5.1486 eV [76, 77].

Again, within the MO theory, the energy of electronic transition in the UV range is estimated by the HOMO-LUMO energy gap, or the band gap. The oscillator strength is related to the dipole transition matrix elements between HOMO and LUMO. The relation between the oscillator strength and transition energy and NLO properties have been established in the literature [78]. When a crystal is exposed to an oscillating electric field through radiation, the field perturbed the electronic distribution. The perturbed electronic state can be expressed as a linear sum of all unperturbed complete set of states. Consequently, the tensor for the frequency dependent NLO properties can be expressed in terms of dipole transition matrix elements between the unperturbed ground state the excited states. We note that this principle is used to calculate the NLO properties in so-called sum-over-state (SOS) method [79]. The detail equation relating the NLO properties and oscillator strength is given in reference 79.

The sketch of computed UV-Visible spectrum represented in Fig. S1 and Fig. S2. The calculation is done in vacuum using optimized geometry from DFT/B3LYP/6311+G(d,p). The

electronic absorption spectra of title compound show an electronic absorption band with maxima at λ_{max} = 252 nm, which is good in agreement with theoretical value (λ_{max} at 245 nm) and this excitation corresponds to transition from highest occupied molecular orbitals (HOMO) and lowest molecular orbitals (LUMO). The absorption wavelength λ (nm), excitation energies E (eV) and oscillator strengths (*f*) for the CSBA molecule computed by same method and results are listed in Table S1.

3.8.Mulliken atomic charge analysis

The Mulliken atomic charge calculations [80] of the CSBA compound performed at DFT/B3LYP method by using 6-311+G(d,p) basic set. From the analysis, it indicates that hydrogen atoms showed positive atomic charges in the range 0.162 to 0.208 a.u., but H18 (0.289), H19 (0.283) and H20 (0.298) atom possess more positive atomic charge value proportional to other hydrogen atoms and were acidic in nature. Due to the presence of more negative atomic charges values on nitrogen atom N4 (-0.485 a.u.) and oxygen atoms O3 (-0.300 a.u.), O5 (-0.219) and O7 (-0.078) net positive atomic charge value on hydrogen atom H18 (0.289), H19 (0.283) and H20 (0.298) may support the formation of hydrogen bond interactions in the solid state.

3.9. Sensitivity towards autoxidation

Predicting shelf life of organic molecules is of importance for practical applications. In these regards it is very important to estimate to what extent organic molecule of interest is sensitive towards the autoxidation mechanism. The dissociation energies for the hydrogen abstraction (H-BDE) of the benzene moiety have been correlated with sensitivity towards autoxidation and the relevant interval of H-BDE values indicating sensitivity towards autoxidation has been determined [81-84]. The importance of H-BDE parameter for biochemical processes has been also established. Namely, it has been demonstrated that the breaking of C-H bonds is very important for the phase I drug metabolism [85]. Another important aspect of applicability of H-BDE parameter is environmental protection and the area of forced degradation. One of the most important mechanisms for degradation of organic pollutants, and especially of pharmaceutical molecules, is oxidation [86]. Therefore, considering the importance of this parameter, we have used it in order to additionally investigate local reactivity of CSBA molecule. H-BDE values of CSBA have been presented in Fig. 8.

It has been established so far that the relevant interval of H-BDE values that indicate sensitivity towards autoxidation is between 70 and 90 kcal/mol [83,84]. Results obtained in this study for H-BDE parameter indicate that CSBA molecule has no H-BDE values that would indicate its sensitivity towards autoxidation mechanism. Namely, all H-BDE values are higher than the upper threshold of 90 kcal/mol. This means that CSBA molecule might be highly stable in the presence of oxygen and therefore could have long shelf life. It also means that its degradation could be difficult under natural conditions, meaning that forced degradation via photo catalysts might be employed for its removal. In the same time the BDE value of carbon-sulphur bond calculated as 43.72 kcal/mol reveals that degradation could initiated by detaching of carbon-sulphur bond.

3.10. Thermal Analysis

The thermal analysis of CSBA compound was done by thermo gravimetric analysis (TGA) and differential thermal analysis (DTA) in nitrogen environment with heating rate 5^{o}C/min up to 1200^{o}C. The spectrum was recorded on EXSTAR TG/DTA 6300 instrument. From the analysis of TGA curve (Fig.9), the primary weight loss of 0.33% over the temperature range of 30^{o}C to 201^{o}C is due to elimination of moisture and other volatile materials. The CSBA decompose occur in three stages, the first from 201°C to 300°C with mass loss of 10.25%, after a major mass loss of 71.91% is observed from 300°C to 400°C and finally 16.49% of mass is lost in the third between 400-600°C. The residual mass of the compound was 0.5%. From the TGA curve, the primary endothermic peak was observed at 255^{o}C reflect the melting point of single crystal and another endothermic peak at 318^{o}C is accountable to the weight loss in TGA curve. The sharpness of the peak reflects the good degree of crystallinity of the compound. From the thermal we concluded that the crystal stable up to 201^{o}C without any decomposition. Hence from the TGA/DTA analysis, it may notice that the present investigated compound is stable and can be used for NLO material upto 201^{o}C.

3.11. Anti-bacterial activity

The synthesized CSBA compound were screened for *in vitro* anti-bacterial activity against gram-positive bacteria (*S. aureus* and *B. cereus*) and gram-negative bacteria (*E. coli* and *P. aeruginosa*) by disc diffusion method using DMSO as a solvent [87]. Zone of inhibition (ZI) in mm for the tested compound was measured after 24-48 h incubation at 37°C for bacteria. Ciprofloxacin was used as a standard drug under similar conditions and compared with the tested

compounds. Control test with solvents were performed for every assay but showed no inhibition of microbial growth. The results revealed that the tested compound exhibited moderate anti-bacterial activity against gram-negative and gram-positive bacterial strains and this could be owing to the presence of sulfonamide moiety and electron-withdrawing chloro groups on the benzoic acid (Table 10).

4. Conclusion

In conclusion, the compound 4-chloro-3-sulfamoylbenzoic acid (CSBA) was synthetized. The explicit structure of CSBA was characterized by SCXRD, FT-IR, FT-Raman and quantum chemical calculations. The calculated geometrical measures were in confirmation with the SCXRD measures and the computed wave numbers were in accord with the experimentally measured wave numbers. The MEP depiction reflected that the negative region confirmed over deprotonated atoms which were possible sites for electrophilic attack and the positive region confirmed over protonated atoms as possible sites for nucleophilic attack. HOMO was localized over whole molecule other than acid group and LUMO was spread over the whole molecule other than the amine group and this reflects that there was a charge transfer process from amine group to acid group. For the titled compound, the second-order hyperpolarizibilitiy (γ) was calculated and found to be 15.01×10^{-36} esu, which is 3.62 times that of the standard NLO material urea. The absence of H-BDE values lesser than 70-85 kcal/mol, which showed that the CSBA compound cannot be treated as sensitive towards autoxidation mechanism. The tested compound showed moderate anti-bacterial activity against gram-negative and gram-positive bacterial strains.

Acknowledgements

The authors are grateful to University Grant Commission-Network Resource Center (UGC-NRC), School of Chemistry, University of Hyderabad for providing computational support. We are also thankful to SAIF, Gauhati University and IIT, Chennai for the analysis support.

References

[1] W.R. Roush, S.L. Gwaltney, J. Cheng, K.A. Scheidt, J.H. McKerrow, Elizabeth Hansell, Vinyl sulfonate esters and vinyl sulfonamides: potent, irreversible inhibitors of cysteine proteases, J. Am. Chem. Soc. 120(42) (1998) 10994-10995.

[2] E. De Clercq, New developments in anti-HIV chemotherapy, Curr. Med. Chem. 8 (2001) 1543-1572

[3] J. Mun, A.A. Jabbar, N.S. Devi, S. Yin, Y. Wang, C. Tan, D. Culver, J.P. Snyder, Van E.G. Meir, M.M. Goodman, Design and in-vitro activities of N-alkyl-N-[(8-R-2,2-

dimethyl-2H-chromen-6-yl)methyl]heteroarylsulfonamides, novel, small-molecule hypoxia inducible factor-1 pathway inhibitors and anticancer agents, J. Med. Chem. 55 (2012) 6738-6750.

[4] N.S. El-Sayed, E.R. El-Bendary, S.M. El-Ashry, M.M. El-Kerdawy, Synthesis and antitumor activity of new sulfonamide derivatives of thiadiazolo[3,2-a]pyrimidines, Eur. J. Med. Chem. 46 (2011) 3714-3720.

[5] J.I. Levin, J.M. Chen, M.T. Du, F.C. Nelson, L.M. Killar, S. Skala, A. Sung, G. Jin, R. Cowling, D. Barone, C.J. March, K.M. Mohler, R.A. Black, J.S. Skotnicki, Anthranilate sulphonamide hydroxamate TACE inhibitors. Part 2: SAR of the acetylenic P1′ group, Bioorg. Med. Chem. Lett. 12(8) (2002) 1199-202.

[6] J.F. Kennedy, M. Thorley, Pharmaceutical Substances, 3rd ed., A. Kleeman, J. Engel, B. Kutscher, D. Reichert, Thieme, Stuttgart, 1999.

[7] D. Vullo, V. De Luca, A. Scozzafava, V. Carginale, M. Rossi, C.T. Supuran, C. Capasso, The extremo-α-carbonic anhydrase from the thermophilic bacterium Sulfurihydrogenibiumazorense is highly inhibited by sulphonamides, Bioorg Med Chem. 21(15) (2013) 4521-5.

[8] Chester M. Himal, Wissam G. Aboul-Saad, J. Agr. Food. Chem. 19(6) (1971) 1175-1180.

[9] K. Chibale, H. Haupt, H. Kendrick, V. Yardley, A. Saravanamuthu, A.H. Fairlamb, S.L. Croft, Antiprotozoal and cytotoxicity evaluation of sulfonamide and urea analogues of quinacrine, Bioorg. & Med. Chem. Lett. 11 (2001) 2655.

[10] A. Hanafy, J. Uno, H. Mitani, Y. Kang, Y. Mikami, In Vitro antifungal activities of sulfa drugs against clinical Isolates of Aspergillus and Cryptococcus species, Jpn. J. Med. Mycol. 48(1) (2007) 47-50.

[11] S.S. Stokes, R. Alber, E.T. Buurman, B. Andrews, A.B. Shapiro, O.M. Green, A.R. McKenzie, L.R. Otterbein,Inhibitors of the acetyltransferase domain of N-acetylglucosamine-1-phosphate-uridylyltransferase/glucosamine-1-phosphate-acetyltransferase (GlmU). Part 2: Optimization of physical properties leading to antibacterial aryl sulfonamides, Bioorg. & Med. Chem. Lett. 23 (2012) 7019-7023.

[12] N. Hirayama, J. Taga, S. Oshima, T. Honjo, Sulfonamide-type di-schiff baseligands as chelate extraction reagents for divalent metal cations, Anal. ChimActa466 (2002) 295-301.

[13] E.G.C. Clarke, A.C. Moffat (Eds.), Clarke's Isolation and Identification of Drugs, The Pharmaceutical Press, London, 1986.

[14] S.C. Chaturvedi, S.H. Mishra, K.L. Bhargava, Indian Drugs 17 (1980) 367.

[15] B.T. Gowda, K. Jyothi, J.D.D. Souza, Z. Naturforsch. 57a (2002) 967.

[16] B.T. Gowda, K. Jyothi, J. Kozisek, H. Fuess, Z. Naturforsch. 58a (2003) 656.

[17] M. Karabacak, M. Cinar, A. Coruh, M. Kurt, Theoretical investigation on the molecular structure, Infrared, Raman and NMR spectra of para-halogen

benzenesulfonamides, 4-X-C6H4SO2NH2 (X = Cl, Br or F), J. Mol. Struct. 919 (2009) 26-33.

[18] K. Govindarasu, E. Kavitha, N. Sundaraganesan, Spectrochim, Acta A 133 (2014) 417-431.

[19] S. Murugavel, V. Vetri velan, D. Kannan, M. Bakthadoss, J. Mol. Struct. 1108 (2016) 150-167.

[20] S. Murugavel, V. Vetri velan, D. Kannan, M. Bakthadoss, J. Mol. Struct. 1115 (2016) 33-54.

[21] E.G. Vega-Hissi, M.F. Andrada, G.N. Zamarbide, M.R. Estrada, F.T. Vert, Theoretical studies on sulphanilamide and derivatives with antibacterial activity: conformational and electronic analysis, J. Mol. Model. 17 (2011) 1317-1323.

[22] F. Yu, J. Ma, D. Bi, Enhanced adsorptive removal of selected pharmaceutical antibiotics from aqueous solution by activated grapheme, Environmental Science and Pollution Research, 22(6) (2015) 4715-4724.

[23] K. Liu, S. Zhang, X. Hu, K. Zhang, A. Roy, G. Yu, Understanding the adsorption of PFOA on MIL-101 (Cr)-based anionic-exchange metal-organic frameworks: comparing DFT calculations with aqueous sorption experiments, Environmental science & technology, 49(14) (2015) 8657-8665.

[24] T. Wang, X.X. Tian, Y.W. Li, J. Wang, M. Beller, H. Jiao, Coverage-dependent CO adsorption and dissociation mechanisms on iron surfaces from DFT computations, ACS Catalysis, 4(6) (2014) 1991-2005.

[25] S. Armaković, S.J. Armaković, S. Koziel, Optoelectronic properties of curved carbon systems, Carbon, 111 (2017) 371-379.

[26] Bruker APEX2, SADABS, SAINT-Plus and XPREPBruker AXS Inc., Madison, Wisconsin, USA2009.

[27] G.M. Sheldrick, A short history of SHELX, ActaCryst. A64 (2008) 112-122.

[28] Gaussian 09, Revision B.01, M.J. Frisch, G.W. Trucks, H.B. Schlegel, G.E. Scuseria, M.A. Robb, J.R. Cheeseman, G. Scalmani, V. Barone, B. Mennucci, G.A. Petersson, H. Nakatsuji, M. Caricato, X. Li, H.P. Hratchian, A.F. Izmaylov, J. Bloino, G. Zheng, J.L. Sonnenberg, M. Hada, M. Ehara, K. Toyota, R. Fukuda, J. Hasegawa, M. Ishida, T. Nakajima, Y. Honda, O. Kitao, H. Nakai, T. Vreven, J.A. Montgomery, Jr., J.E. Peralta, F. Ogliaro, M. Bearpark, J.J. Heyd, E. Brothers, K.N. Kudin, V.N. Staroverov, T. Keith, R. Kobayashi, J. Normand, K. Raghavachari, A. Rendell, J.C. Burant, S.S. Iyengar, J. Tomasi, M. Cossi, N. Rega, J.M. Millam, M. Klene, J.E. Knox, J.B. Cross, V. Bakken, C. Adamo, J. Jaramillo, R. Gomperts, R.E. Stratmann, O. Yazyev, A.J. Austin, R. Cammi, C. Pomelli, J.W. Ochterski, R.L. Martin, K. Morokuma, V.G. Zakrzewski, G.A. Voth, P. Salvador, J.J. Dannenberg, S. Dapprich, A.D. Daniels, O. Farkas, J.B. Foresman, J.V. Ortiz, J. Cioslowski, D.J. Fox, Gaussian, Inc., Wallingford CT, 2010.

[29] R. Dennington, T. Keith, J. Millam, GaussView, version 5, Semichem Inc.,Shawnee Mission, KS, 2009.

[30] J.B. Foresman, Pittsburg, PA, in: E. Frisch (Ed.), Exploring Chemistry with Electronic Structure Methods: a Guide to Using Gaussian, 1996.

[31] M.A. Spackman, D. Jayatilaka, Hirshfeld surface analysis, CrystEngComm. 11 (2009) 19-32.

[32] F.L. Hirshfeld, Bonded-Atom Fragments for Describing Molecular Charge Densities, Theor. Chim. Acta 44 (1977) 129-138.

[33] H.F. Clausen, M.S. Chevallier, M.A. Spackman, B.B. Iversen, Three new co-crystals of hydroquinone: crystal structures and Hirshfeld surface analysis of intermolecular interactions, New J. Chem. 34 (2010) 193-199.

[34] A.L. Rohl, M. Moret, W. Kaminsky, K. Claborn, J.J. McKinnon, B. Kahr, Hirshfeld surfaces identify inadequacies in computations of intermolecular interactions in crystals: pentamorphic 1, 8-dihydroxyanthraquinone, Cryst. Growth Des. 8 (2008) 4517-4525.

[35] A. Parkin, G. Barr, W. Dong, C.J. Gilmore, D. Jayatilaka, J.J. McKinnon, M.A. Spackman, C.C. Wilson, Comparing entire crystal structures: structural genetic fingerprinting, CrystEngComm. 9 (2007) 648-652.

[36] M.A. Spackman, J.J. McKinnon, Fingerprinting intermolecular interactions in molecular crystals, CrystEngComm. 4 (2002) 378-392.

[37] S.K. Wolff, D.J. Grimwood, J.J. McKinnon, D. Jayatilaka, M.A. Spackman, Crystal Explorer 2.0; University of Western Australia, Australia, 2012.

[38] K. Tamagawa, T. Iijima, M. Kimura, Molecular structure of benzene, J. Mol. Struct. 30 (1976) 243-253.

[39] P. Krishna Murthy, V. Suneetha, Stevan Armaković, Sanja J. Armaković, C. Van Alsenoy, P.A. Suchetan, R. Sreenivasa Rao, Synthesis, characterization and computational study of the newly synthetized sulfonamide molecule, J. Mol. Struct. 1153 (2018) 212-229.

[40] P. Krishna Murthy, G. Krishna Swamy, Stevan Armaković, Sanja J. Armaković, P.A. Suchetan, Nivedita R Desai, V. Suneetha, R. Sreenivasa Rao, G. Bhargavi, D. B. Aruna Kumar, Structural and spectroscopic characterization, reactivity study and charge transfer analysis of the newly synthetized 2-(6-hydroxy-1-benzofuran-3-yl) acetic acid, J. Mol. Struct. 1162 (2018) 81-95.

[41] P. Krishna Murthy, Y. Sheena Mary, V. Suneetha, C.Y. Panicker, Stevan Armaković, Sanja J. Armaković, L. Giri, P.A. Suchetan, C. Van Alsenoy, Towards the new heterocyclic based pharmaceutical molecule: synthesis, characterization and reactivity study, J. Mol. Struct. 1137 (2017) 589-605.

[42] N.P.G. Roges, A Guide to the Complete Interpretation Of Infrared Spectra of Organic Structures, John Wiley And Sons, New York, 1994.

[43] N.R. Colthup, L.H. Daly, S.E. Wiberly, Introduction to Infrared and Raman Spectroscopy, Academic Press, New York, 1975.

[44] G. Socrates, Infrared characteristics group frequencies, John Wiley and Sons, New York, 1981.

[45] M. Silverstein, G.C. Basseler, C. Morill, Spectrometric identification of organic compounds, Wiley, New York, 1981.

[46] G. Varsanyi, Assignment of vibrational spectra of 700 benzene derivatives, Wiley, New York, 1974.

[47] E.D. Glendening A.E. Reed, J.E. Carpenter, F. Weinhold, NBO Version 3.1, Gaussian Inc., Pittsburgh, PA, 2003.

[48] E.D. Glendening, C.R. Landis, F. weinhold, Natural bond method, WIREs. Comp. Mol. Sci. 2 (2012) 1-42.

[49] M.N. Tahir, M. Khalid, A. Islam, S.M.A. Mashhadi, A.A.C. Braga, Facile synthesis, single crystal analysis, and computational studies of sulphanilamide derivatives, J. Mol. Struct. 1127 (2017), 766-776.

[50] S. Naseem, M. Khalid, M.N. Tahir, M.A. Halim, A.A.C. Braga, M.M. Naseer, Z. Shafiq, Synthesis, structural, DFT studies, docking and antibacterial activity of a xanthene based hydrazone ligand, J. Mol. Struct. 1143 (2017) 235-244.

[51] D.S. Chemia, J. Zysss, Nonlinear Optical Properties of Organic Molecules and Crystals, Acadamic Press, Orlando, FL, 1987.

[52] D.S. Bradsshow, D.L. Andrews, J. Nonlinear Opt. Phys. Matter, 18 (2009) 285-299.

[53] C. Adant, M. Dupuis, J.L. Bredas, Ab initio study of the nonlinear optical properties of urea, electron correlation and dispersion affects, Int. J. Quantum Chem. 56 (2004) 497-507.

[54] P.K. Murthy, C. Valverde, V. Suneetha, S. Armaković, S.J. Armaković, N.U. Rani, N.V. Naidu, An analysis of structural and spectroscopic signatures, the reactivity study of synthetized 4,6-dichloro-2-(methylsulfonyl)pyrimidine: A potential third-order nonlinear optical material, J. Mol. Struct. 1186 (2019) 263–275. doi:10.1016/j.molstruc.2019.03.021.

[55] J.M.F. Custodio, R.R. Ternavisk, C.J.S. Ferreira, A.S. Figueredo, G.L.B. Aquino, H.B. Napolitano, C. Valverde, B. Baseia, Using the Supermolecule Approach To Predict the Nonlinear Optics Potential of a Novel Asymmetric Azine, J. Phys. Chem. A. 123 (2019) 153–162. doi:10.1021/acs.jpca.8b07872.

[56] J.M.F. Custodio, G.D.C. D'Oliveira, F. Gotardo, L.H.Z. Cocca, L. De Boni, C.N. Perez, L.J.Q. Maia, C. Valverde, F.A.P. Osório, H.B. Napolitano, Chalcone as Potential Nonlinear Optical Material: A Combined Theoretical, Structural, and Spectroscopic Study, J. Phys. Chem. C. 123 (2019) 5931–5941. doi:10.1021/acs.jpcc.9b01063.

[57] C. Valverde, Í.N. Ribeiro, J.V.B. Soares, B. Baseia, F.A.P. Osório, Prediction of the Linear and Nonlinear Optical Properties of a Schiff Base Derivatives via DFT, Adv. Condens. Matter Phys. 2019 (2019) 1–12. doi:10.1155/2019/8148392.

[58] C. Valverde, F.A.P. Osório, T.L. Fonseca, B. Baseia, DFT study of third-order nonlinear susceptibility of a chalcone crystal, Chem. Phys. Lett. 706 (2018) 170–174. doi:10.1016/j.cplett.2018.06.001.

[59] C. Valverde, S.A. de Lima e Castro, G.R. Vaz, J.L. de Almeida Ferreira, B. Baseia, F.A.P. Osório, Third-Order Nonlinear Optical Properties of a Carboxylic Acid Derivative, Acta Chim. Slov. 65 (2018) 739–749. doi:10.17344/acsi.2018.4462.

[60] J.M.F. Custodio, F.G. Santos, W.F. Vaz, C.E.P. Cunha, R.G. Silveira, M.M. Anjos, C.E.M. Campos, G.R. Oliveira, F.T. Martins, C.C. da Silva, C. Valverde, B. Baseia, H.B. Napolitano, Molecular structure of hybrid imino-chalcone in the solid state: X-ray diffraction, spectroscopy study and third-order nonlinear optical properties, J. Mol. Struct. 1157 (2018) 210–221. doi:10.1016/j.molstruc.2017.12.023.

[61] A.N. Castro, F.A.P. Osório, R.R. Ternavisk, H.B. Napolitano, C. Valverde, B. Baseia, Theoretical investigations of nonlinear optical properties of two crystalline acetamides structures including polarization effects of their environment, Chem. Phys. Lett. 681 (2017) 110–123. doi:10.1016/j.cplett.2017.05.066.

[62] C. Valverde, W.F. Vaz, J.M.F. Custodio, V.S. Duarte, P.S. Carvalho-Jr, A.S. Figueredo, G.L.B. de Aquino, B. Baseia, H.B. Napolitano, The solid state structure and environmental polarization effect of a novel asymmetric azine, New J. Chem. 41 (2017) 11361–11371. doi:10.1039/C7NJ00618G.

[63] C. Valverde, R.F.N. Rodrigues, D.F.S. Machado, B. Baseia, H.C.B. de Oliveira, Effect of the crystalline environment on the third-order nonlinear optical properties of L-arginine phosphate monohydrate: a theoretical study, J. Mol. Model. 23 (2017) 122. doi:10.1007/s00894-017-3274-3.

[64] L.R. Almeida, M.M. Anjos, G.C. Ribeiro, C. Valverde, D.F.S. Machado, G.R. Oliveira, H.B. Napolitano, H.C.B. de Oliveira, Synthesis, structural characterization and computational study of a novel amino chalcone: a potential nonlinear optical material, New J. Chem. 41 (2017) 1744–1754. doi:10.1039/C5NJ03214H.

[65] J. Custodio, C. Moreira, C. Valverde, G. de Aquino, B. Baseia, H. Napolitano, Hirshfeld Surfaces and Nonlinear Optics on Two Conformers of a Heterocyclic Chalcone, J. Braz. Chem. Soc. 29 (2017) 258–268. doi:10.21577/0103-5053.20170136.

[66] B. Baseia, F. Osório, L. Lima, C. Valverde, Effects of Changing Substituents on the Non-Linear Optical Properties of Two Coumarin Derivatives, Crystals. 7 (2017) 158. doi:10.3390/cryst7060158.

[67] W.F. Vaz, J.M.F. Custodio, R.G. Silveira, A.N. Castro, C.E.M. Campos, M.M. Anjos, G.R. Oliveira, C. Valverde, B. Baseia, H.B. Napolitano, Synthesis, characterization, and third-order nonlinear optical properties of a new neolignane analogue, RSC Adv. 6 (2016) 79215–79227. doi:10.1039/C6RA14961H.

[68] G.C. Ribeiro, L.R. Almeida, H.B. Napolitano, C. Valverde, B. Baseia, Polarization effects on the third-order nonlinear optical properties of two polymorphs of enamine derivative, Theor. Chem. Acc. 135 (2016) 244. doi:10.1007/s00214-016-1999-1.

[69] A.N. Castro, L.R. Almeida, M.M. Anjos, G.R. Oliveira, H.B. Napolitano, C. Valverde, B. Baseia, Theoretical study on the third-order nonlinear optical properties and structural

characterization of 3-Acetyl-6-Bromocoumarin, Chem. Phys. Lett. 653 (2016) 122–130. doi:10.1016/j.cplett.2016.04.070.

[70] Rodrigues, Rosemberg FN, Leonardo R. Almeida, Florisberto G. dos Santos, Paulo S. Carvalho Jr, Wanderson C. de Souza, Kleber S. Moreira, Gilberto LB de Aquino, Clodoaldo Valverde, Hamilton B. Napolitano, Basílio Baseia, Solid state characterization and theoretical study of non-linear optical properties of a Fluoro-N-Acylhydrazide derivative, PloS one 12, no. 4 (2017): e0175859.

[71] J.S. Murray, K. Sen, Molecular Electrostatic Potentials, Concepts and Applications, Elsevier, Amsterdam, 1996.

[72] E. Scrocco, J. Tomasi, Electronic Molecular Structure, Reactivity and Intermolecular Forces: An Euristic Interpretation by Means of Electrostatic Molecular Potentials, Adv. Quantum Chem. 11 (1979) 115-193.

[73] R.G. Parr, W. Yang, Density functional approach to the frontier-electron theory of chemical reactivity, J. Am. Chem. Soc. 106 **(**1984) 4049-4050.

[74] P.W. Ayers, M. Levy, Perspective on "Density functional approach to the frontier-electron theory of chemical reactivity", Theor. Chem. Acc. 103 (2000) 353-360.

[75] P. Geerlings, F. De Proft, W. Langenaeker, Conceptual Density Functional Theory, Chem. Rev. 103 (2003) 1793-1874.

[76] T.A. Koopmans, Uber die zuordnung von wellenfunktionen und eigenwertenzu den einzelnenelektroneneines atoms, Physica 1 (1993) 104-113.

[77] R.J. Parr, L.V. Szentpaly, S. Liu, Electrophilicity index, J. Am. Chem. Soc. 121 (1999) 1922-1924.

[78] S. D. Bella, second order nonlinear optical properties of transition metal complexes, Chem. Soc. Rev. 30 (2001)355-366.

[79] K. Sasagane, F. Aiga, R. Itoh, Higher order response theory based on the quasienergy derivatives: The derivation of the frequency dependent polarizabilities and hyperpolarizabilities, J. Chem. Phys. 99(1993)3738.

[80] R.S. Mulliken, Electronic population analysis on LCAO-MO molecular wave function, J. Chem. Phys. 23 (1955) 1833-1840.

[81] T. Andersson, A. Broo, E. Evertsson, Prediction of Drug Candidates' Sensitivity Toward Autoxidation: Computational Estimation of C-H Dissociation Energies of Carbon□Centered Radicals, Journal of pharmaceutical sciences, 103(7) (2014) 1949–1955. DOI: 10.1002/jps.23986

[82] P. Lienard, J. Gavartin, G. Boccardi, M. Meunier, Predicting drug substances autoxidation, Pharmaceutical research, 32(1) (2015) 300–310. DOI: 10.1007/s11095-014-1463-7

[83] J.S. Wright, H. Shadnia, L.L. Chepelev, Stability of carbon□centered radicals: Effect of functional groups on the energetics of addition of molecular oxygen, Journal of computational chemistry, 30(7) (2009), 1016–1026. DOI: 10.1002/jcc.21124

[84] G. Gryn'ova, J.L. Hodgson, M.L. Coote, Revising the mechanism of polymer autooxidation, Organic & biomolecular chemistry, 9(2) (2011) 480–490. DOI:10.1039/C0O B00 596G

[85] K.L. Drew, J. Reynisson, The impact of carbon–hydrogen bond dissociation energies on the prediction of the cytochrome P450 mediated major metabolic site of drug-like compounds, European journal of medicinal chemistry, 56 (2012) 48–55. DOI: 10.1016/j.ejmech.2012.08.017

[86] S.W. Hovorka, C. Schöneich, Oxidative degradation of pharmaceuticals: Theory, mechanisms and inhibition, Journal of pharmaceutical sciences, 90(3) (2001) 253–269. DOI: 10.1002/1520-6017(200103)90:3<253::AID-JPS1>3.0.CO;2-W

[87] A.L. Barry, Antimicrobial susceptibility test, Principles and Practices, Lea and Febiger, Philadelphia, 1987.

Figure caption(s)

Scheme -1. Synthesis of 4-chloro-3-sulfamoylbenzoic acid.

Figure 1. Fourier transformed Infrared spectrum of 4-chloro-3-sulfamoylbenzoic acid.

Figure 2. Fourier transformed Raman spectrum of 4-chloro-3-sulfamoylbenzoic acid.

Figure 3. The *ORTEP* diagram of the 4-chloro-3-sulfamoylbenzoic acid with thermal ellipsoids drawn at 50% probability with optimized geometry.

Fig. 4(a). Formation of a dimer via O-H…O hydrogen bonds; b. A view of the complex two dimensional architecture formed by two N-H…O hydrogen bonds; c. Another view of the 2D architecture displaying zig-zag nature.

Fig. 4(b). A partial view of the three dimensional grid like architecture formed by C-H…O intermolecular interactions.

Fig. 5. Hishfeld surface analysis of 4-chloro-3-sulfamoylbenzoic acid.

Fig. 6. MEP plot of 4-chloro-3-sulfamoylbenzoic acid.

Fig. 7. HOMO-LUMO plots of 4-chloro-3-sulfamoylbenzoic acid.

Fig. 8. BDE for all single acyclic bonds of 4-chloro-3-sulfamoylbenzoic acid.

Fig. 9. DTA/TGA graph of 4-chloro-3-sulfamoylbenzoic acid.

Table caption(s)

Table 1. Crystallographic data and structure refinement parameters of 4-chloro-3-sulfamoylbenzoic acid.

Table 2. Geometric parameters for hydrogen bonds and other intermolecular contacts (Å,°) operating in the crystal structures of 4-chloro-3-sulfamoylbenzoic acid.

Table 3. Geometrical parameters of the 4-chloro-3-sulfamoylbenzoic acid.

Supplementary Information

Table 1.
Crystal data and structure refinement for 4-chloro-3-sulfamoylbenzoic acid.

CCDC number	1920201
Empirical formula	$C_7H_6O_4SClN$
Formula weight	235.64
Temperature/K	296.15
Crystal system	monoclinic
Space group	$P2_1/c$
a/Å	4.9576(3)
b/Å	6.0315(3)
c/Å	29.8923(16)
α/°	90
β/°	92.628(3)
γ/°	90
Volume/Å^3	892.89(8)
Z	4
ρ_{calc}g/cm^3	1.753
μ/mm^{-1}	0.647
F(000)	480.0
Crystal size/mm^3	0.24 × 0.22 × 0.19
Radiation	MoKα (λ = 0.71073)
2Θ range for data collection/°	6.892 to 60.062
Index ranges	$-6 \leq h \leq 6$, $-8 \leq k \leq 8$, $-41 \leq l \leq 41$
Reflections collected	10070
Independent reflections	2584 [R_{int} = 0.0257, R_{sigma} = 0.0221]
Data/restraints/parameters	2584/3/140
Goodness-of-fit on F^2	1.241
Final R indexes [I>=2σ (I)]	R_1 = 0.0419, wR_2 = 0.1037
Final R indexes [all data]	R_1 = 0.0443, wR_2 = 0.1052
Largest diff. peak/hole / e Å^{-3}	0.37/-0.49

Table 2.
Geometric parameters for hydrogen bonds and other intermolecular contacts (Å, °) operating in the crystal structures of 4-chloro-3-sulfamoylbenzoic acid.

D-H…A	D-H	H…A	D…A	D-H…A
O5-H18...O3^{i}	0.82	1.83	2.6331	167
N4-H19...O7^{ii}	0.85	2.28	3.0467	150
N4-H20...O7^{iii}	0.84	2.21	3.0219	163
C15-H16...O5^{iv}	0.93	2.60	3.5155	169
i: -1-x,1-y,-z; ii: -1+x,y,z; iii: 1-x,1/2+y,1/2-z; iv: 1+x,1+y,z				

Table 3.
Geometrical parameters of the 4-chloro-3-sulfamoylbenzoic acid.

Bond length (Å) DFT/XRD			
C8-O3	1.20772/1.252	C8-O5	1.35213/1.273
C8-C9	1.48971/1.484	C9-C10	1.39614/1.388
C10-C12	1.39308/1.394	C12-C17	1.39985/1.396
C15-C17	1.39370/1.386	C13-C15	1.38752/1.378
C13-C9	1.39718/1.389	C12-S2	1.82275/1.7800
S2-O6	1.45598/1.4258	S2-N4	1.66847/1.5884
S2-O7	1.45235/1.4374	C17-Cl1	1.75083/1.7200
Bond angle (º) DFT/XRD			
O6-S2-O7	122.4/119.2	C12-S2-N4	107.6/107.4
O6-S2-N4	105.7/108.0	O7-S2-N4	106.7/107.2
C12-S2-O6	105.7/105.8	C12-S2-O7	107.8/108.5
O3-C8-O5	122.8/123.2	C10-C12-C17	119.4/119.4
C10-C9-C13	119.7/119.8	C12-C17-C15	120.3/120.1
C15-C17-Cl1	117.5/116.8	C13-C9-C8	118.1/119.6
C12-C17-Cl1	122.1/122.9	C10-C9-C8	122.1/120.4
Torsion angle (º) DFT/XRD			
O6-S2-C12-C10	-8.2/12.7	O7-S2-C12-C17	-53.3/-42.4
O6-S2-C12-C17	174.0/-171.6	O7-S2-C12-C10	124.2/141.8
N4-S2-C12-C10	-120.9/-102.4	N4-S2-C12-C17	61.4/73.1
O3-C8-C9-C13	0.1/2.2	O5-C8-C9-C13	-179.7/-177.
O3-C8-C9-C10	-179.7/-179.7	O5-C8-C9-C10	0.3/0.3

Table 4.
Calculated scaled wave numbers, observed IR and Raman bands and assignment of 4-chloro-3-sulfamoylbenzoic acid.

B3LYP/6-311G++(d, p)			ν(IR)(cm^{-1})	ν(Raman)(cm^{-1})	Assignment
ν (cm^{-1})	IR intensity	Raman activity			
3623	125.1003	157.5832	-	-	OH(100)
3495	44.9905	28.6368	3401	3403	NH(50)
3383	32.8958	91.3757	3281	3279	NH(50)
3096	13.5854	39.0879	3093	-	νCH(99)
3086	0.906	143.906	-	3084	νCH(51)
3073	0.4339	39.8359	3072	-	νCH(51)
1722	423.2576	138.0385	1721	1720	νC=O(84)
1562	67.4577	121.6563	-	1563	νC=C(18)
1535	7.3653	11.8495	1532	1531	νC=C(23)
1520	44.5197	3.6388	-	1518	δNH_2(83)
1354	47.8115	2.28	1352		1351
1315	163.3855	22.5635	1313	1310	νOH(32)
1286	153.7678	7.4928	1284	1285	νSO_2(42)
1155	238.7422	59.0964	1145	-	δCH(10) νOH(44)
1119	4.6545	4.3601	1115	1116	δCH(15) νC=C(15)
1090	122.5881	18.3156	-	1090	νSO_2(27)
1071	92.3408	4.749	-	1072	νSO_2(17), νC=C(11)
1066	108.3526	2.8884	-	-	δCH(10)
1041	4.7781	5.2138	1042	1043	δNH(83)
1003	80.2009	20.3098	-	-	ring breathing (27)
965	0.0047	0.0774	-	-	δCH(45)
831	12.2233	0.2571	832	833	δCH(48)
825	74.4512	18.1962	-	-	νCS(15) νSN(16)
782	20.2025	10.8642	-	785	νSN(56)
749	62.9529	0.11	745	747	δCH(13)
674	45.7856	11.3182	676	675	δC=O(17)
646	21.5916	1.4169	641		δC=O(23) νCCl (12)
587	375.3294	2.265	587	585	δNH(19)
550	45.1653	2.1073	548	551	νCCl (17) δC=O(18)
513	6.3932	2.7591	-	514	δSO_2(15)
460	33.6788	0.9877	-	458	δSO_2(23)
432	10.6856	1.7013	-	430	δSO_2(17)

393	11.9518	3.0486	-	389	$\delta SO_2(15)$

[a]ν-stretching; δ-in-plane deformation and out-of-plane deformation; τ-torsion; potential energy distribution is given in brackets (%) in the assignment column.

Table 5.
Second-order perturbation theory analysis of Fock matrix in NBO basis corresponding to the intramolecular bonds of the title compound

Donor(i)	Type	ED/e	Acceptor(j)	Type	ED/e	E(2)[a]	E(j)-E(i)[b]	F(i,j)[c]
C9-C13	π	1.61680	O3-C8	π*	0.25203	21.28	0.27	0.07
			C10-C12	π*	0.34137	25.76	0.27	0.07
			C15-C17	π*	0.36846	20.33	0.26	0.06
C10-C12	π	1.67641	C9-C13	π*	0.35519	15.45	0.30	0.061
			C15-C17	π*	0.36846	21.82	0.28	0.070
C15-C17	π	1.65447	C9-C13	π*	0.35519	21.26	0.30	0.072
			C10-C12	π*	0.34137	16.84	0.029	0.062
LP Cl1	3	1.91353	C15-C17	π*	0.36846	10.86	0.32	0.057
LP O3	π	1.84478	O5-C8	σ*	0.09752	33.42	0.61	0.130
-	-	-	C8-C9	σ*	0.06950	19.20	0.68	0.104
LP O5	π	1.81825	O3-C8	σ*	0.25203	47.46	0.34	0.115
LP O6	π	1.81069	S2-N4	σ*	0.23778	14.38	0.42	0.070
-	-	-	S2-C12	σ*	0.21798	16.83	0.43	0.077
LP O6	3	1.79016	S2-O7	σ*	0.16267	21.75	0.57	0.101
LP O7	3	1.77264	S2-N4	σ*	0.23778	13.38	0.41	0.066
-	-		S2-O6	σ*	0.15139	21.28	0.56	0.100

[a] E(2) means energy of hyper-conjugative interactions (stabilization energy in kcal/mol)
[b] Energy difference (a.u) between donor and acceptor i and j NBO orbitals
[c] F(i,j) is the Fock matrix elements (a.u) between i and j NBO orbitals

Table 6.
NBO results showing the formation of Lewis and non-Lewis orbitals.

Bond(A-B)	ED/e[a]	EDA%	EDB%	NBO	s%	p%
πC9-C13	1.61680	55.08	44.92	0.7422(SP1.00)C+	0.00	99.98
	-0.27460			0.6702(SP1.00)C	0.00	99.95
πC10-C12	1.67641	43.13	56.87	0.6567(SP1.00)C+	0.00	99.94
	-0.29066			0.7541(SP99.99)C	0.01	99.97
πC15-C17	1.65447	49.04	50.96	0.7003(SP1.00)C+	0.00	99.95
	-0.29473			0.7138(SP1.00)C	0.00	99.97
σO3-C8	1.99694	65.64	34.36	0.8102($sp^{1.41}$)O+	41.33	58.29
	-1.09393			0.5862($sp^{1.95}$)C	33.82	66.07
πO3-C8	1.98305	69.41	30.59	0.8332(sp1.00)O+	0.00	99.66
				0.5530(SP1.00)C	0.00	99.81
σ S2-N4	1.97879	36.93	63.07	0.6077($sp^{3.53}$)S+	21.62	76.58
	-0.78334	-	-	0.7942($sp^{3.13}$)N	24.21	75.73
σ S2-O6	1.98453	33.77	66.23	0.5811($sp^{2.65}$)S+	26.97	71.51
	-0.98076			0.8138($sp^{3.00}$)O	24.88	74.66
σ S2-O7	1.98313	33.80	66.20	0.5814($sp^{2.58}$)S+	27.51	70.95
	-0.98141			0.8136($sp^{3.03}$)O	24.72	74.82
σ S2-C12	1.96399	44.82	55.18	0.6695($sp^{3.07}$)S+	24.17	74.28
	-0.69792			0.7428($sp^{3.07}$)C	24.58	75.38
σ O5-C8	1.99570	68.54	31.46	0.8279($sp^{1.92}$)O+	34.20	65.73
	-0.94645			0.5609($sp^{2.64)}$C	27.43	72.32
σ C8-C9	1.97469	47.23	52.77	0.6872($sp^{1.58}$)C+	38.70	61.24
	-0.69086			0.7264($sp^{2.30}$)C	30.32	69.64
n3 Cl1	1.96795	-	-	0.7138(sp1.00)C+	0.00	99.95
	-0.34059			0.7003(sp1.00)C+	0.00	99.97

n2 O3	1.84478	-	-	$sp^{1.00}$	0.00	99.74
	-0.27310					
n2 O5	1.81825	-	-	$sp^{1.00}$	0.00	99.88
	-0.34427					
n2 O6	1.81069	-	-	$sp^{1.00}$	0.00	99.70
	-0.29976					
n3 O6	1.79016	-	-	$sp^{99.97}$	0.07	99.61
	-0.29669					
n3 O7	1.77264	-	-	$sp^{99.99}$	0.02	99.66
	-0.29282					

[a] ED/e is expressed in a.u.

Table 7

The electric dipole moment (μ), linear polarizability (α) and second order hyper polarizability (γ) of the asymmetric unit of title compound by CAM-B3LYP/6-311G+(d) in the case static.

Parameter	Value	Parameter	esu($x10^{-24}$)	Parameter	esu($x10^{-36}$)
μ_x	2.89	α_{xx}	17.16	γ_{xxxx}	10.41
μ_y	3.42	α_{xy}	-3.55	γ_{yyyy}	7.46
μ_z	0.17	α_{yy}	16.53	γ_{zzzz}	16.83
μ_o	4.48	α_{xz}	4.93	γ_{xxyy}	2.90
		α_{yz}	1.34	γ_{xxzz}	7.27
		α_{zz}	21.70	γ_{yyzz}	4.15
		$<\alpha>$	18.46	$<\gamma>$	12.67
		$\Delta\alpha$	11.83		

Table 8.
The linear polarizability (α) and second order hyper polarizability (γ) of the cell unit of title compound by CAM-B3LYP/6-311G+(d) in the case static.

Parameter	esu($x10^{-24}$)	Parameter	esu($x10^{-36}$)
$\alpha_{xx}/4$	16.65	$\gamma_{xxxx}/4$	9.89
$\alpha_{xy}/4$	-0.42	$\gamma_{yyyy}/4$	6.93
$\alpha_{yy}/4$	16.29	$\gamma_{zzzz}/4$	25.44
$\alpha_{xz}/4$	5.47	$\gamma_{xxyy}/4$	2.78
$\alpha_{yz}/4$	-0.72	$\gamma_{xxzz}/4$	8.41
$\alpha_{zz}/4$	23.92	$\gamma_{yyzz}/4$	5.20
$<\alpha>/4$	18.95	$<\gamma>/4$	15.01
$\Delta\alpha/4$	12.14		

Table 9. The Fukui reactive index (FRI) for nucleophilic (f^+), electrophilic (f^-) and radical (f^0) reactivities of different atom.

FRI	Cl	S	O3	N	O5	O6	O7	C8	C9	C10	C12	C13	C15	C17
f^+	0.113	0.021	0.098	0.027	0.047	0.037	0.039	0.080	0.068	0.040	0.043	0.079	0.050	0.087
f^-	0.182	0.015	0.077	0.054	0.025	0.046	0.057	0.023	0.095	0.034	0.054	0.062	0.045	0.075
f^0	0.148	0.018	0.088	0.041	0.036	0.042	0.048	0.052	0.064	0.037	0.049	0.071	0.048	0.081

Table 10. Anti-bacterial activity of CSBA compound against bacterial pathogens

Concentration of sample (40 mg/mL)	Anti-bacterial activity (in mm)			
	Gram-positive		Gram-negative	
	S. aureus	*B. cereus*	*E. coli*	*P. aeruginosa*
Title compound	15.4	13.9	10.7	12.2
Ciprofloxacin (30µg/disc)	24.5	25.1	27.6	31.8
Control (10% DMSO)	-	-	-	-

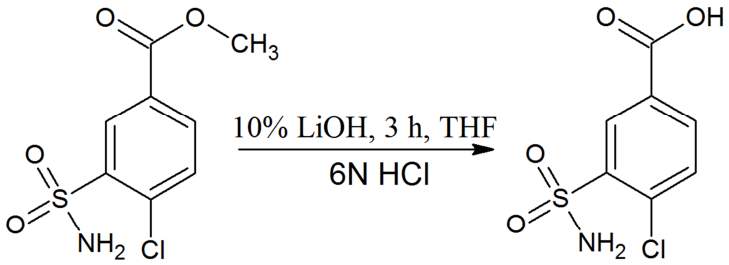

Scheme 1: Synthesis of 4-chloro-3-sulfamoylbenzoic acid

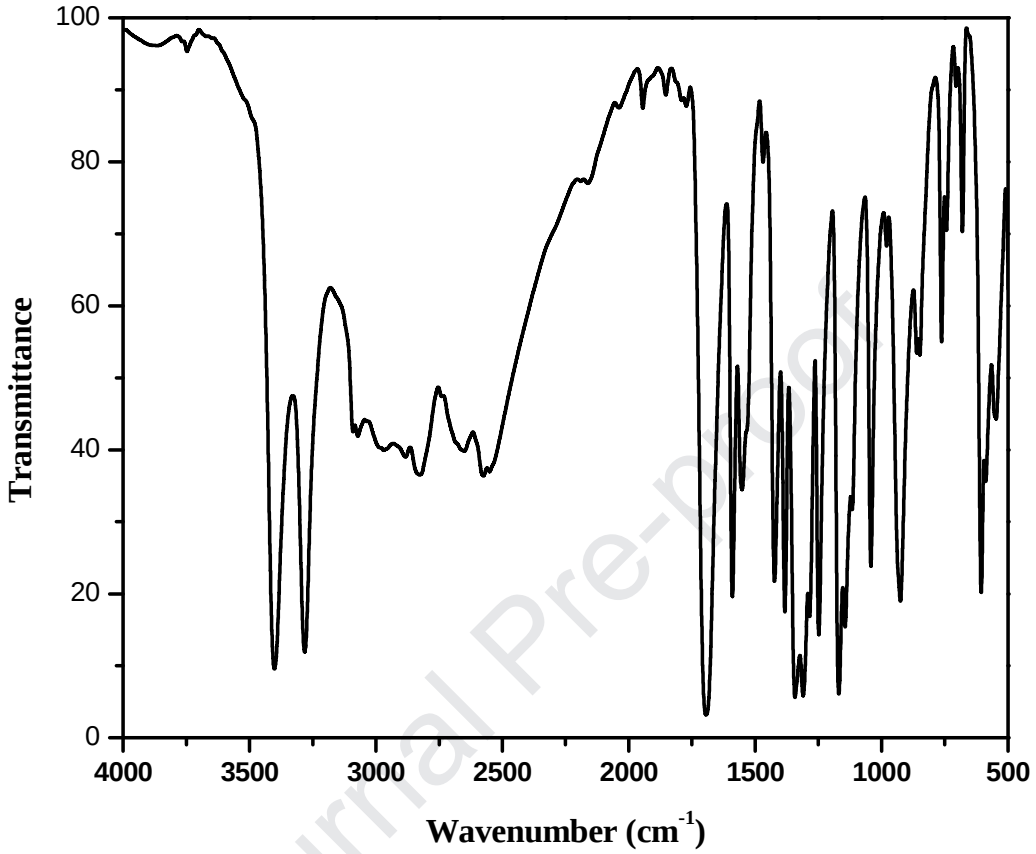

Fig. 1. Fourier transformed Infrared spectrum of 4-chloro-3-sulfamoylbenzoic acid.

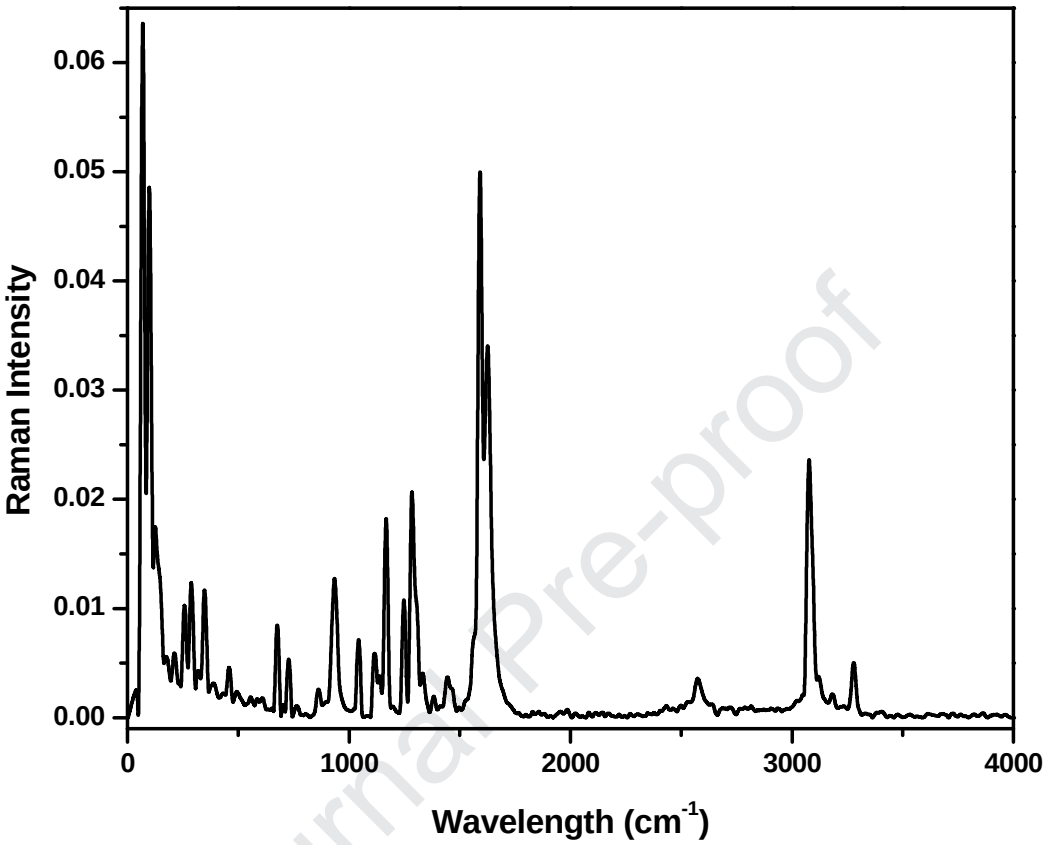

Fig. 2. Fourier transformed Raman spectrum of 4-chloro-3-sulfamoylbenzoic acid.

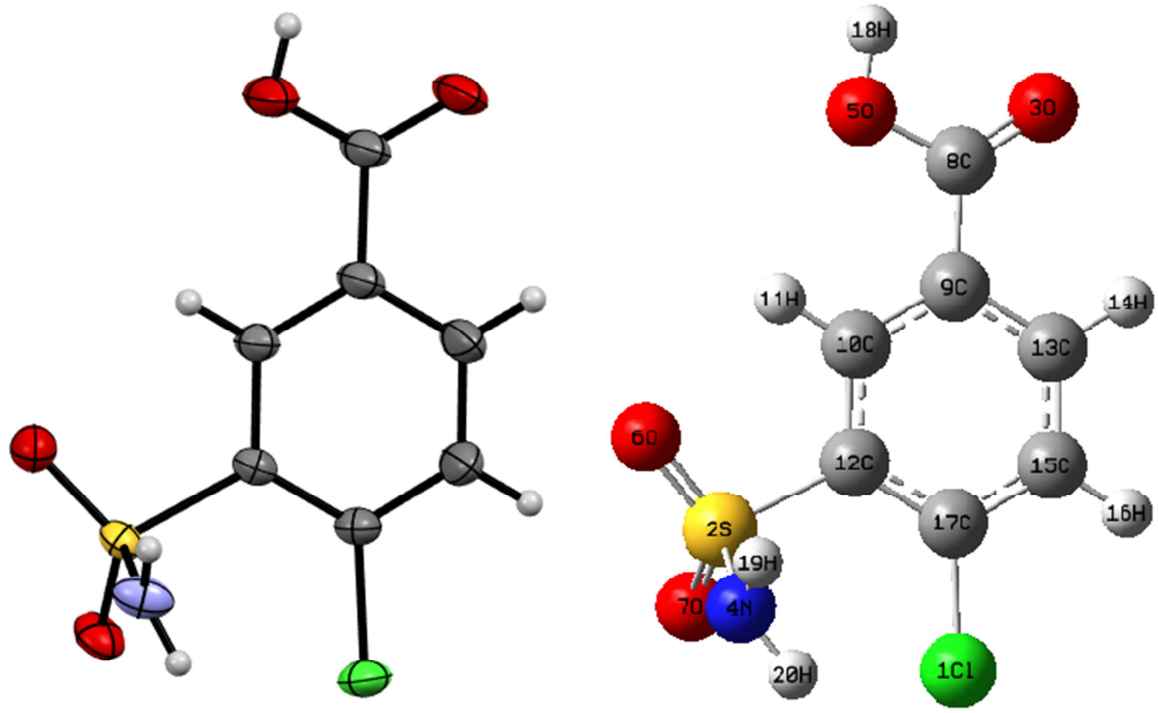

Fig. 3. The *ORTEP* diagram of the 4-chloro-3-sulfamoylbenzoic acid with thermal ellipsoids drawn at 50% probability with optimized geometry.

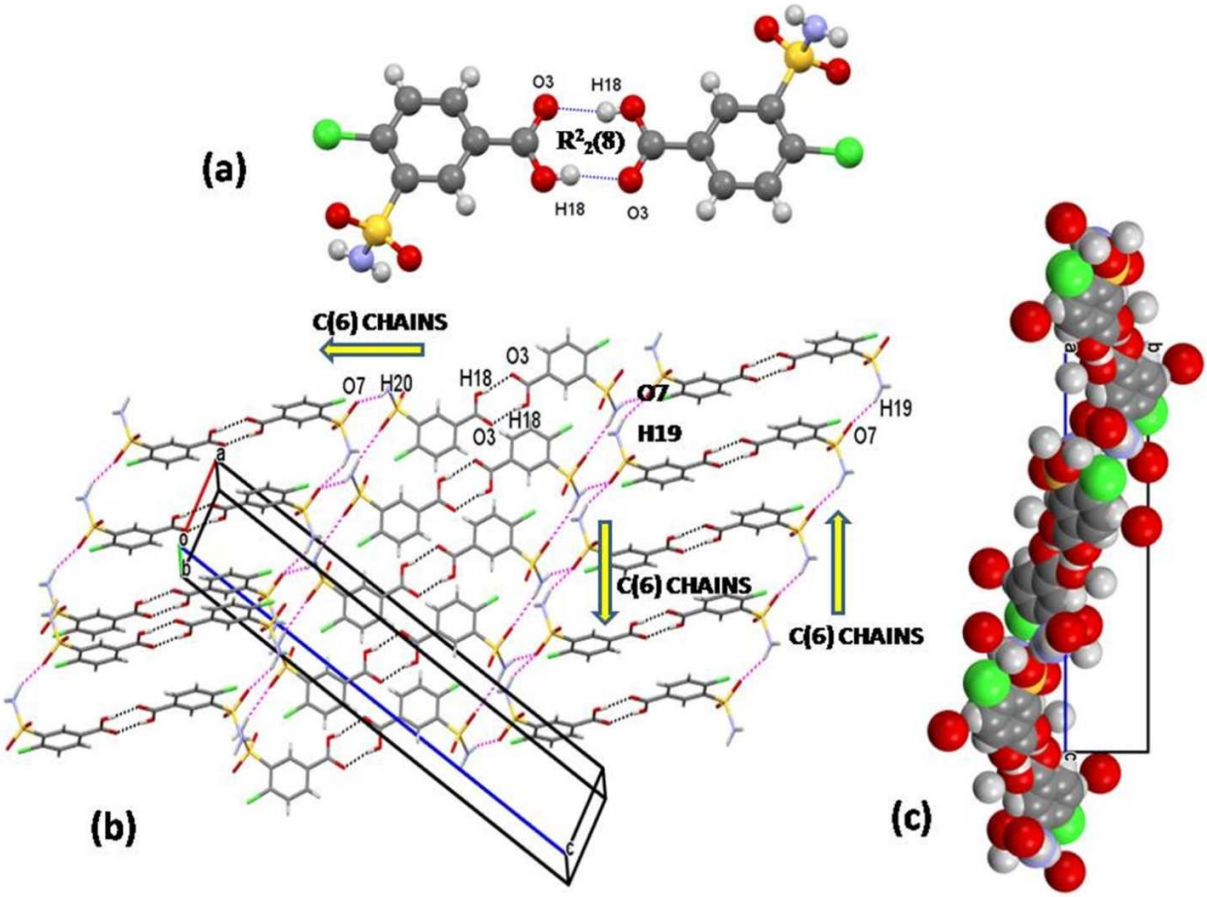

Fig. 4(a). Formation of a dimer via O-H…O hydrogen bonds; b. A view of the complex two dimensional architecture formed by two N-H…O hydrogen bonds; c. Another view of the 2D architecture displaying zig-zag nature.

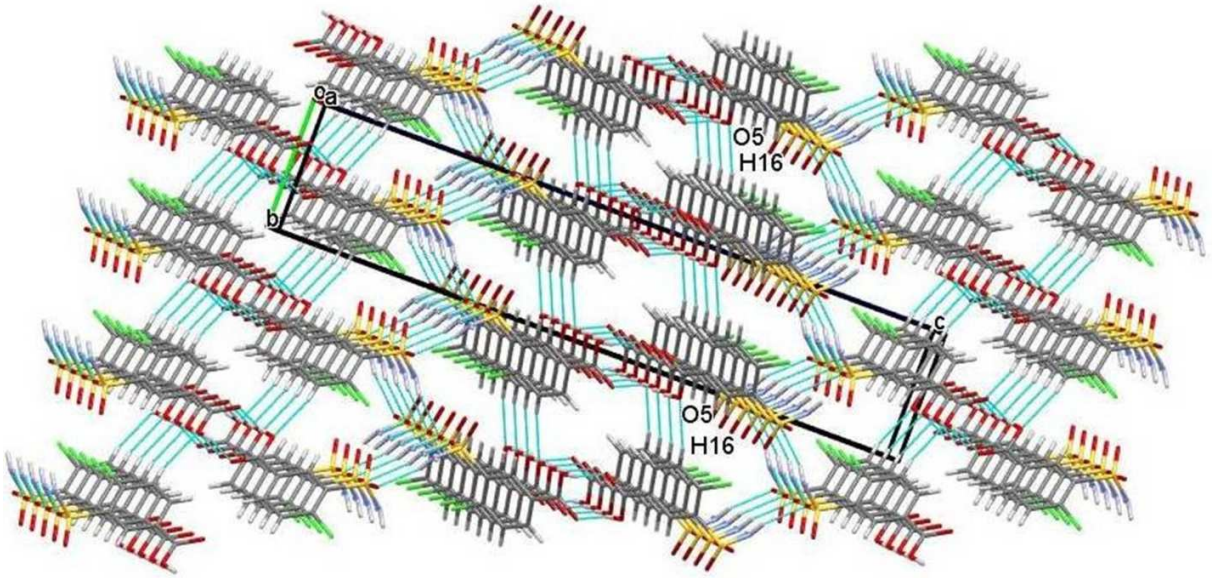

Fig. 4(b). A partial view of the three dimensional grid like architecture formed by C-H…O intermolecular interactions.

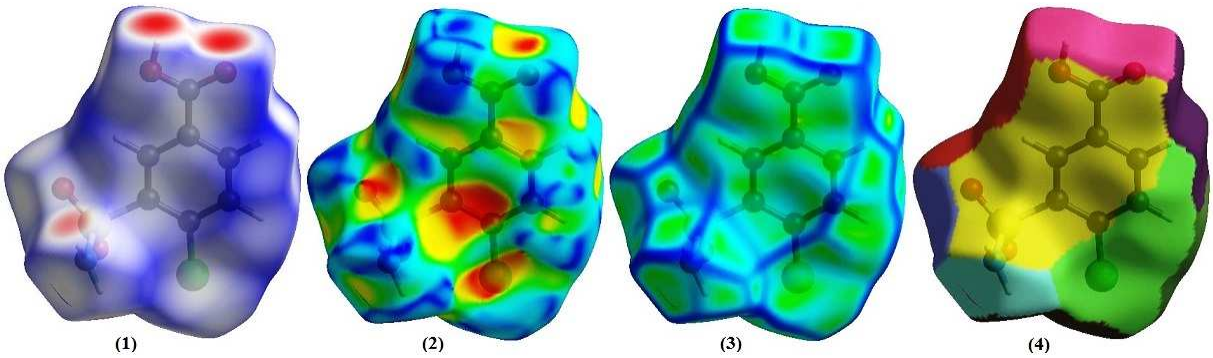

(a) Hirshfeld surfaces of CSBA: d_{norm} (1), *shape index* (2), *curvedness* (3), *fragment patch* (4).

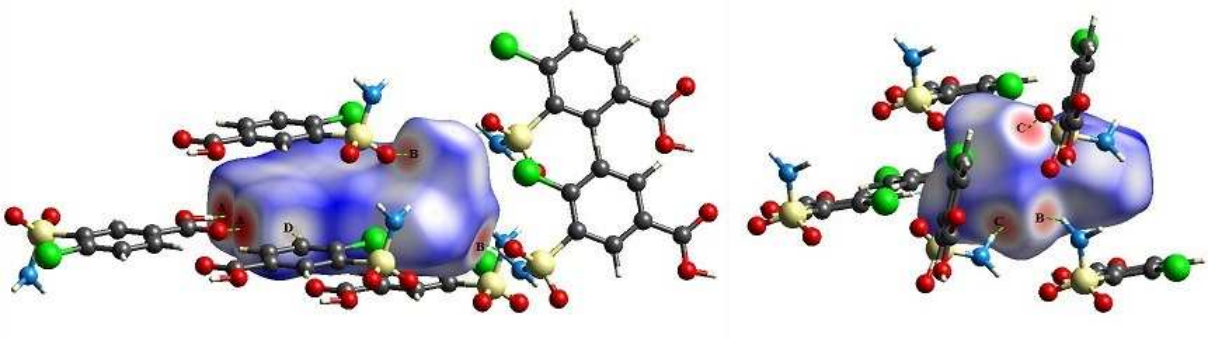

(b) View of O---H interactions.

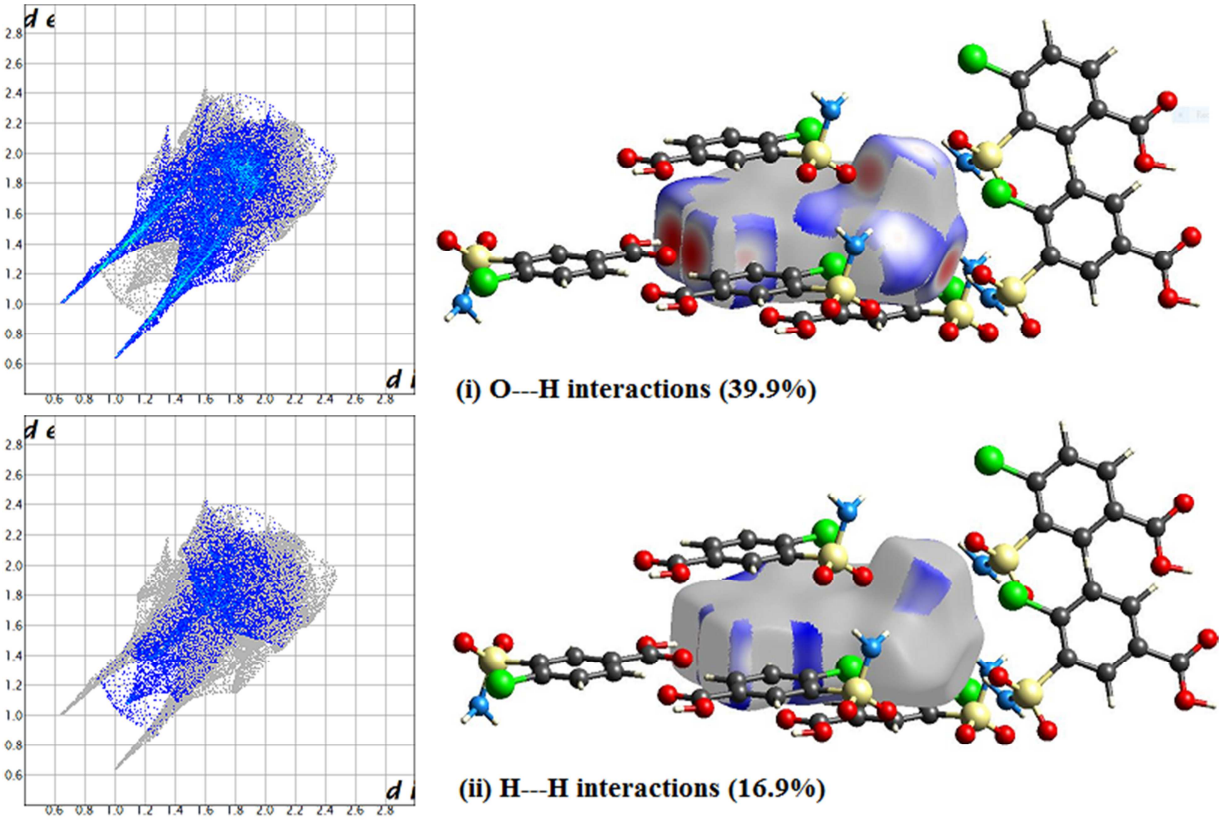

(c) Finger print plots of the CSBA compound and major interactions visualized with percentage (i) O---H interactions (39.9%) and H---H interactions (16.9%).

Fig. 5. Hishfeld surface analysis of 4-chloro-3-sulfamoylbenzoic acid.

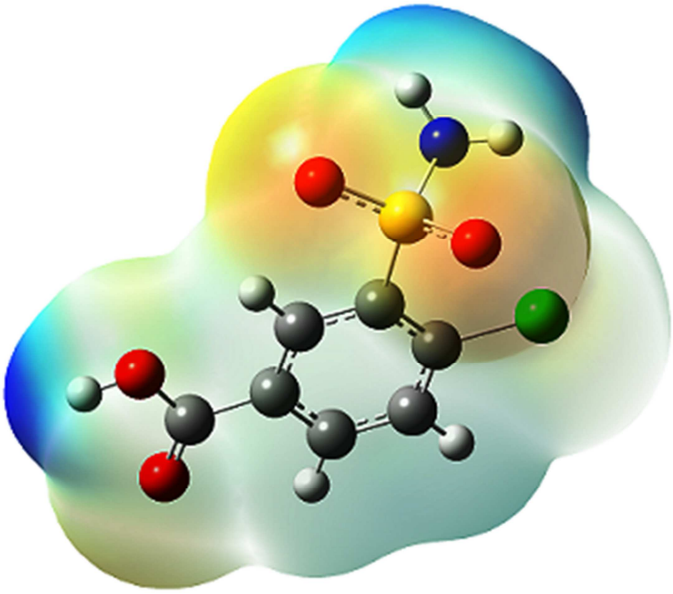

Fig. 6. MEP plot of 4-chloro-3-sulfamoylbenzoic acid.

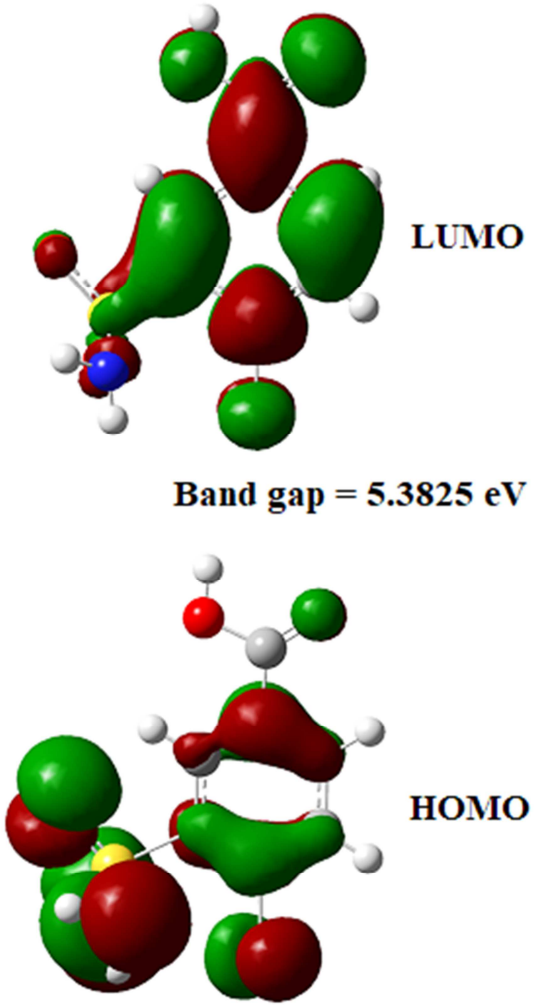

Fig. 7. HOMO-LUMO plots of 4-chloro-3-sulfamoylbenzoic acid.

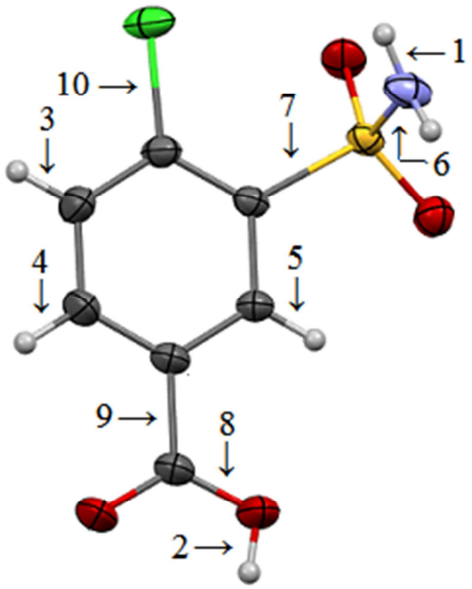

Bond	BDE [kcal/mol]
1.	104.64
2.	105.28
3.	112.31
4.	113.20
5.	112.88
6.	97.67
7.	43.72
8.	104.66
9.	99.82
10.	85.54

Fig. 8. BDE for all single acyclic bonds of 4-chloro-3-sulfamoylbenzoic acid.

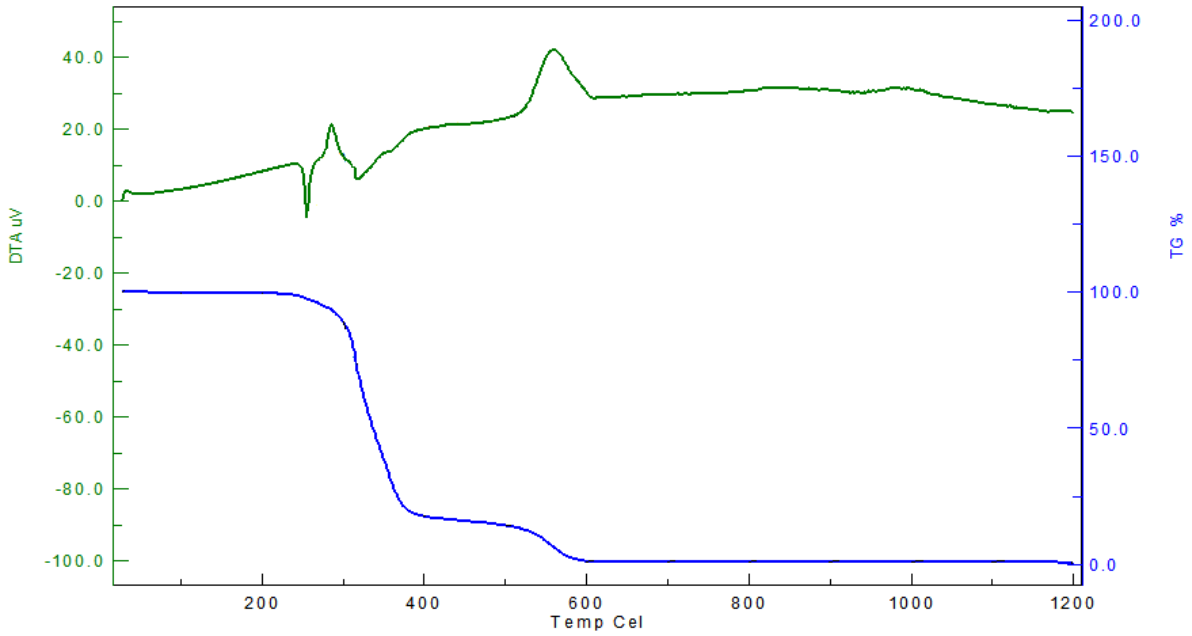

Fig. 9. DTA/TGA graph of 4-chloro-3-sulfamoylbenzoic acid.

Highlights

- The explicit structure of title compound was authenticated by single crystal X-ray diffraction, vibrational and electronic spectroscopic signatures.
- Most reactive sites are identified.
- MEP, BDE and Fukui function have been discussed in detail.
- The complete vibrational assignments were performed on the basic of the potential energy distribution (PED).